

Iraqi National Journal of Earth Science

www.earth.mosuliournals.com



Geochemistry and Genesis of Zubair Shales (Lower Cretaceous) in Rumaila Oilfield, Southern Iraq

Rana A. Ali 1* D, Thamer A. Mahdi ²D

^{1,2} Department of Geology, College of Science, University of Baghdad, Baghdad, Iraq.

Article information

Received: 22- June-2024

Revised: 03- Aug -2024

Accepted: 16-Sep -2024

Available online: 01- Oct – 2025

Keywords: Black Shale

Organic Matter Enrichment

Paleoproductivity

Paleoredox Environment

Correspondence: Name: Rana A. Ali

Email:

rana.ali@sc.uobaghdad.edu.iq

ABSTRACT

Exploration and development of shale oil and gas resources depend on understanding the mechanisms that influence the buildup of organicrich shale. In shallow marine facies, the development of organic-rich sediments is largely dependent on the sedimentary environment. The black shale is the main lithology forming the reservoir in the Zubair Formation. The discovery of silica origin, and the differentiation between euxinic sulphuretted and anoxic ferruginous conditions, continue to require further study. First, the geochemical features of Zubair oil shales are examined using geochemical data collected from two wells, R167 and Ru4, in the northern and southern Rumaila oilfields in Basrah, Southern Iraq. Next, the provenance, depositional basin, and evolution of the paleoenvironment are addressed. Lastly, the primary controlling factor of organic matter enrichment is identified. The findings demonstrate that Zubair shales are able to be separated into two units: organic-rich and organic-low shales, with average total organic carbon (TOC) contents of 13.5, 9.04, and 2.39% for R167 and Ru4, respectively. High concentrations of SiO2, V, Ni, Zn, Sr, Zr, Ba, and the distribution of various rare earth elements also distinguish the organic-rich shales. Compared to the organic-low shales, the organicrich shales have a significantly higher proportion of biological quartz and a lower terrigenous input. In the organic-rich shales, the paleoclimate is warm, humid, and of low salinity, while the organiclow shales are cold, dry, and of high salinity. The organic- low shales exhibit an elevated stagnant level with suboxic to oxic conditions and lower paleoproductivity. In contrast, the organic-rich shales exhibit a comparatively lower stagnant level with euxinic to anoxic conditions. Oil shales accumulate in a semi-stagnant basin. The three-stage environmental evolution model demonstrates that paleo-productivity, redox conditions, and sea level fluctuation have a strong causal connection.

DOI: 10.33899/earth.2024.150904.1299, ©Authors, 2025, College of Science, University of Mosul. This is an open access article under the CC BY 4.0 license (http://creativecommons.org/licenses/by/4.0/).

جيوكيمائية ونشأة صخور السجيل لتكوين زبير (العصر الطباشيري الاسفل) في حقل الرميلة النفطي، جنوبي العراق

رنا عباس علي 1* أن ثامر عبدالله مهدي 2 أن عباس علي 1

201 قسم علوم الأرض، كلية العلوم، جامعة بغداد، بغداد، العراق.

الملخص

يعتمد استكشاف وتطوير موارد النفط والغاز الصخريين على فهم الآليات التي تؤثر على تراكم السجيل الغني بالمواد العضوية. وفي المناطق البحرية الضحلة، يعتمد تطور الرواسب الغنية بالمواد العضوية إلى حد كبير على البيئة الرسوبية. السجيل الأسود هو التركيبة الصخربة الرئيسة التي تشكل الخزان في تكوين زبير. إن اكتشاف أصل السيليكا، والتمييز بين ظروف نقص الأكسجين الكبربتيدية والحديدية، لا يزال يتطلب المزيد من الدراسة. أولاً، تم فحص الخصائص الجيوكيميائية للسجيل في تكوبن زبير باستخدام البيانات الجيوكيميائية التي تم جمعها من بئربن هما R167 و Ru4 في حقول نفط الرميلة الشمالية والجنوبية في البصرة، جنوبي العراق. بعد ذلك، تم تناول المصدر والحوض الترسيبي وتطور البيئة القديمة. وأخيرًا، تم تحديد العامل المتحكم الأساسي في إغناء المادة العضوية. أظهرت النتائج أن السجيل في تكوين زبير يمكن فصله إلى وحدتين: السجيل الغني عضوبًا والسجيل منخفض المواد العضوبة، يبلغ متوسط إجمالي محتوى الكاربون العضوى 13.5 (TOC) و9.04 و2.39% لكل من R167 وRu4 على التوالي. يتميز السجيل الغنى أيضًا بالمواد العضوية بتراكيز عالية من Zr ،Sr ،Zn ،Ni ،V ،SiO2، Ba، وتوزيع متباين للعناصر الأرضية النادرة. بالمقارنة مع السجيل العضوى المنخفض، فإن السجيل الغني بالمواد العضوية يحتوى على نسبة أعلى بكثير من الكوارتز البيولوجي ومدخلات أقل من الترسبات الارضية. يكون المناخ القديم دافئًا ورطبًا ومنخفض الملوحة في السجيل الغني بالمواد العضوبة، في حين أن السجيل منخفض المواد العضوبة بارد وجاف وعالى الملوحة. يُظهر السجيل العضوي المنخفض مستوى راكدًا مرتفعًا مع ظروف من نقص الأكسجين والكبربتيد إلى وفرة الأكسجين وانخفاض الإنتاجية القديمة. في المقابل، فإن السجيل الغني بالمواد العضوية يُظهر مستوىً راكدًا أقل نسبيًا مع ظروف من نقص الأكسجين والكبريتيد إلى انعدام الأوكسجين. يتراكم السجيل في أحواض شبه راكدة. يوضح نموذج التطور البيئي ثلاثي المراحل أن الإنتاجية القديمة، وظروف الأكسدة والاختزال، وتقلبات مستوى سطح البحر لها علاقة سببية قوية.

معلومات الارشفة

تاريخ الاستلام: 22- يونيو-2024 تاريخ المراجعة: 03- اغسطس-2024 تاريخ المراجعة: 03- اغسطس-2024 تاريخ القبول: 16- سبتمبر -2024 الكلمات المفتاحية: الكلمات المفتاحية: الصخر الزيتي الاسود الاغناء بالمواد العضوية الانتاجية القديمة والاختزال القديمة

المراسلة:

الاسم: رنا عباس على

Email:

rana.ali@sc.uobaghdad.edu.iq

DOI: 10.33899/earth.2024.150904.1299, @Authors, 2025, College of Science, University of Mosul. This is an open access article under the CC BY 4.0 license (http://creativecommons.org/licenses/by/4.0/)

Introduction

Due to its excellent reservoir qualities, the Lower Cretaceous Zubair oil shales are considered a significant reservoir in the southern regions of Iraq and in some neighboring countries. Given that the shale intervals comprise certain REE and pyrite, this demonstrates a reductive and acidic depositional environment. This is important to point out that the shale sections indicate the source rock characteristics in the formation, where organic-rich shale (ORS) is primarily developed (Idan et al., 2014). The primary focus layer for shale oil discovery, according to investigation execution, is the ORS of oil shales, which originated in a deep shelf alongside a high total organic carbon (TOC) value as well as a substantial shale thickness. Primarily, the paleoenvironment is studied using the main, trace, and rare earth elements of inorganic geochemistry methods. Some immobile elements, like Sc, Th, Hf, Zr, and La, can be transferred from the region of provenance, where they still retain the traces of the source region (Chen et al., 2019). Due to their differentiation in different conditions, certain redox-sensitive elements found in sedimentary rocks, such as Cr, Co, Th, U, Ni, Mo, and V, are

frequently used to denote redox features (Yan et al., 2018; Doner et al., 2018). Additionally, nutrient elements like Ni, Zn, Cu, and Ba ingested by marine organisms and then maintained in sediments along with the biogenic components of the elements as typical replacements for expressing the paleo-productivity (Shen et al., 2014). According to earlier studies, the Zubair shales in Rumaila (North and South) oilfields were deposited in anoxic conditions with significant primary productivity during a semi-restricted deep basin setting (Alsultan et al., 2021). The primary silica sources in oil shale are terrigenous siliciclastic input as well as biogenic silica (Zhang et al., 2021). They both show a rising reverse trend that is thought to be connected to sea level changes, and the subtropical paleoclimate transitioned from a warm, humid climate to a few periods of dry, cold climate with little precipitation. In the Mesopotamian basin, the Zubair shale was deposited in an environment with insufficient hydrodynamics, deep water, and poor oxygen levels (Al-Azzawi, 2012), which relates to the mechanism of enrichment with organic matter. Oxygen deficiency gave way to high productivity as the primary variable governing the organic matter formation of Zubair oil shales in the Rumaila oilfields. Paleo-productivity and paleo-redox conditions have both an impact on the Zubair shales' organic matter enrichment. In contrast, paleo-redox conditions are primarily responsible for organic matter accumulation during sea level modifications. The current work aims to interpret the paleo-environment, depositional site, and provenance by analyzing the TOC, major-, trace-, and REE concentrations of the oil shales along with their comprehensive geochemical properties. Additionally, the primary regulating element of organic matter enrichment is identified. The study, as a whole, offers a theoretical foundation for additional oil shale exploration and the growth of the Zubair oil shales.

Geological setting

Rumaila oilfield is situated 50 km west of Basra Governorate. The field is located between 47°00'- 47°30'E longitudes and 30°00'-30°45'N latitudes (Fig. 1A). The Rumaila is the largest oilfield in Iraq and the sixth in the world, with estimated oil reserves of 17 billion barrels. It was discovered in 1953 and put into production in 1972 (Al-Ameri et al., 2010). The siliciclastic sediments of the Zubair Formation were sourced from the eroded Arabian Shield, which was uplifted during the Jurassic (Late Kimmerian) movement. Deltas across the foreland of the Lower Cretaceous geosyncline carried these clasts to the sea. The Zubair Formation was deposited during the growth of the Alpine geosyncline basin and the continent's gradual uplift (Buday, 1980).

The Zubair Formation is made up of siliciclastic facies deposited in backshore, delta plain, and delta front environments. The succession of the Zubair Formation is subdivided into transgressive, high-stand, and low-stand systems tracts (Davies et al., 2002) (Fig. 1B). In southern Iraq, the lower and upper boundaries of the Zubair Formation are conformable (Buday, 1980). Lithologically, the Zubair Formation is subdivided into the following members: 1-Upper shale member; 2-Upper sandstone member; 3-Middle shale member; 4 Lower sandstone members; and 5 Lower shale members.

The stratigraphic sequence of the Zubair Formation was deposited during transgressiveand highstand systems tracts (TST and HST) (Davies et al., 2002), with the possible effect of lowstand systems tract (LST) in the upper sand member only. Maximum flooding surfaces occur in shale members (Fig. 1B). The upper Zubair Formation portion exposed a shallower area of shale-dominated rocks with high levels of pyrite and organic matter.

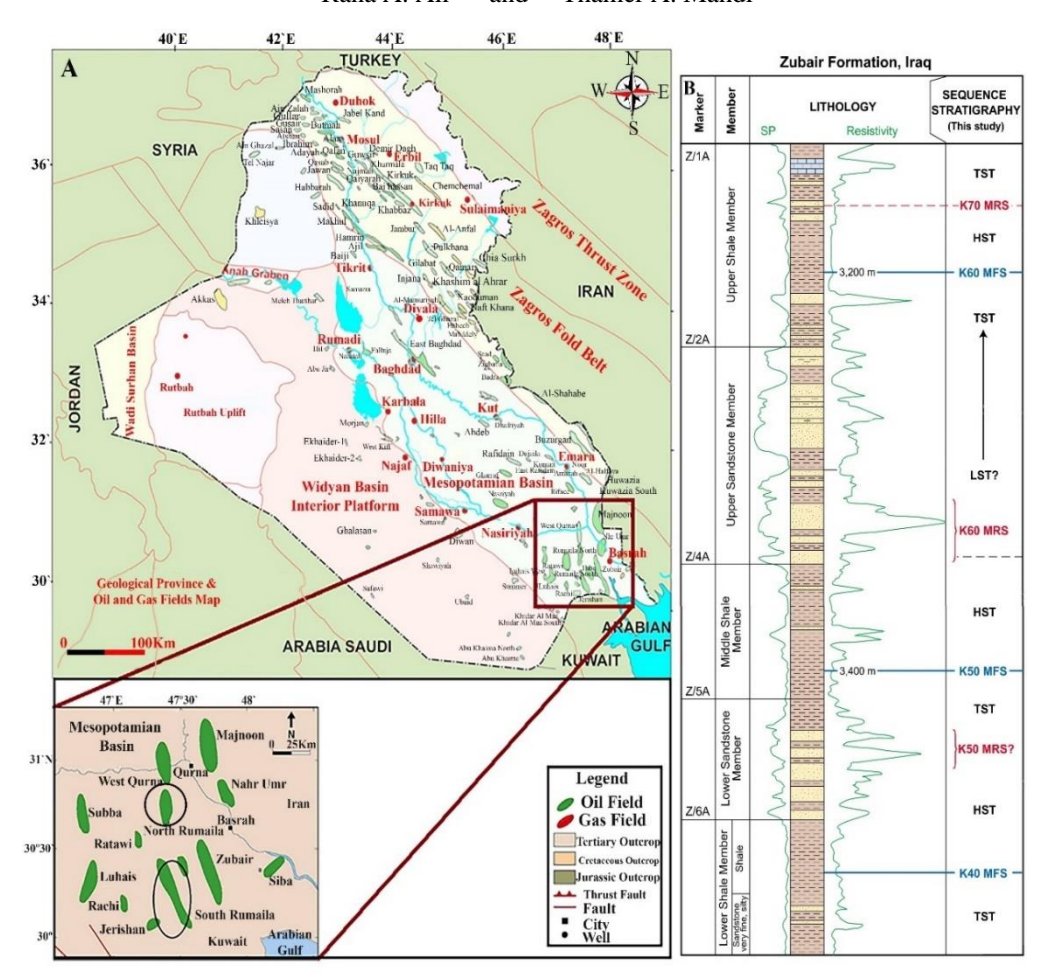


Fig. 1. (A) Location map of Iraq's oil fields, including north and south Rumaila oilfields (adapted from Al-Ameri et al., 2010). (B) Sequence stratigraphy, lithology, and member distribution of the Zubair Formation in southern Iraq (Davies et al., 2002).

Materials and Methods

Samples and Analytical Methods

The typical wells with high oil contents in the study area are R167 and Ru4 of Rumaila north and Rumaila south oilfields, respectively. The study's target samples are located within the main shale members. For all the R167 cores, the ORS samples have a main lithology of black or grey-black shale, and for the majority of samples of well Ru4. The main lithology of the organic-low shale (OLS) cores of well Ru4 is dark-grey sandstone interbedded with shale. From the shale members of the Zubair Formation, a total of 12 core samples were obtained from wells R167 and Ru4. The TOC is evaluated using a CHNS (Perkin-Elemer) tester. XRF is used to examine major elements. The concentrations of trace elements and REE are measured using an atomic absorption spectrometer (SHIMADZU PG-990).

Data presentation

The enrichment factor (EF), which is calculated using the formula (1), is applied to assess the degree of element enrichment in Zubair oil shales (McLennan, 2001).

$$EF = (i/Al)_{sample} / (i/Al)_{PAAS}$$
 (1)

where: *i* is the element *i* concentration, which is normalized using the Post-Archean Australian Shale (*PAAS*).

According to the PAAS standard, EF < 1, 1 < EF < 3, and EF > 3 are generally regarded as depletion, medium enrichment, and evident enrichment, respectively.

Both terrestrial and biological components make up the element concentration in sediments. Due to their chemical stability and low solubility in water, the elements Al and Ti

are used as markers of the terrestrial input in oil shale. The following formula is used to subtract the element's biogenic portion (Wang et al., 2019a):

$$E_{xs} = E_{Sample} - Al_{Sample} \times (E/Al)_{PAAS}$$
 (2)

where: E_{xs} stands for the element E's biogenic component; and E_{Sample} and Al_{Sample} , respectively, are the contents of elements E and Al measured in the sample. The PAAS's element E to Al ratio is $(E/Al)_{PAAS}$.

A common index that reflects redox conditions and historical changes in sea level is the cerium anomaly (8Ce). The formula below is used to calculate the value of 8Ce (He et al., 2019):

$$\delta Ce = Ce_N / (La_N \times Pr_N)^{1/2} \tag{3}$$

where: N reflects PAAS normalized in the formulas mentioned above.

Positive &Ce values above (one) denote suboxic conditions, while negative &Ce values (below 0.95) denote euxinic conditions. Paleo-productivity in oil shale is expressed by the proxies of TOC, Ni/Al, and $Cu_{xs} + Ni_{xs} + Zn_{xs}$. The rate of deposition of oil shale can be measured with the proxy of La_n/Yb_n (n symbolizes chondrite normalization). A lower La_n/Yb_n value denotes a relatively high sedimentation rate.

Results

TOC Concentration

According to the analysis results (Table 1, Table 2, and Fig. 2), the TOC values of the wells R167 and Ru4 range from 8.8 to 16.8% (average 13.5%); and 0.72 to 25.5% (average 6.23%), respectively. The ORS displays high TOC values for wells R167 and Ru4 that range from 4.24 to 25.5% (average 8.96%), while the TOC average for OLS is 0.75%. The TOC values for the OLS (samples Ru4-3, Ru4-6, Ru4-7, and Ru4-11) exhibit noticeably lower values, ranging from 0.72 to 0.78%.

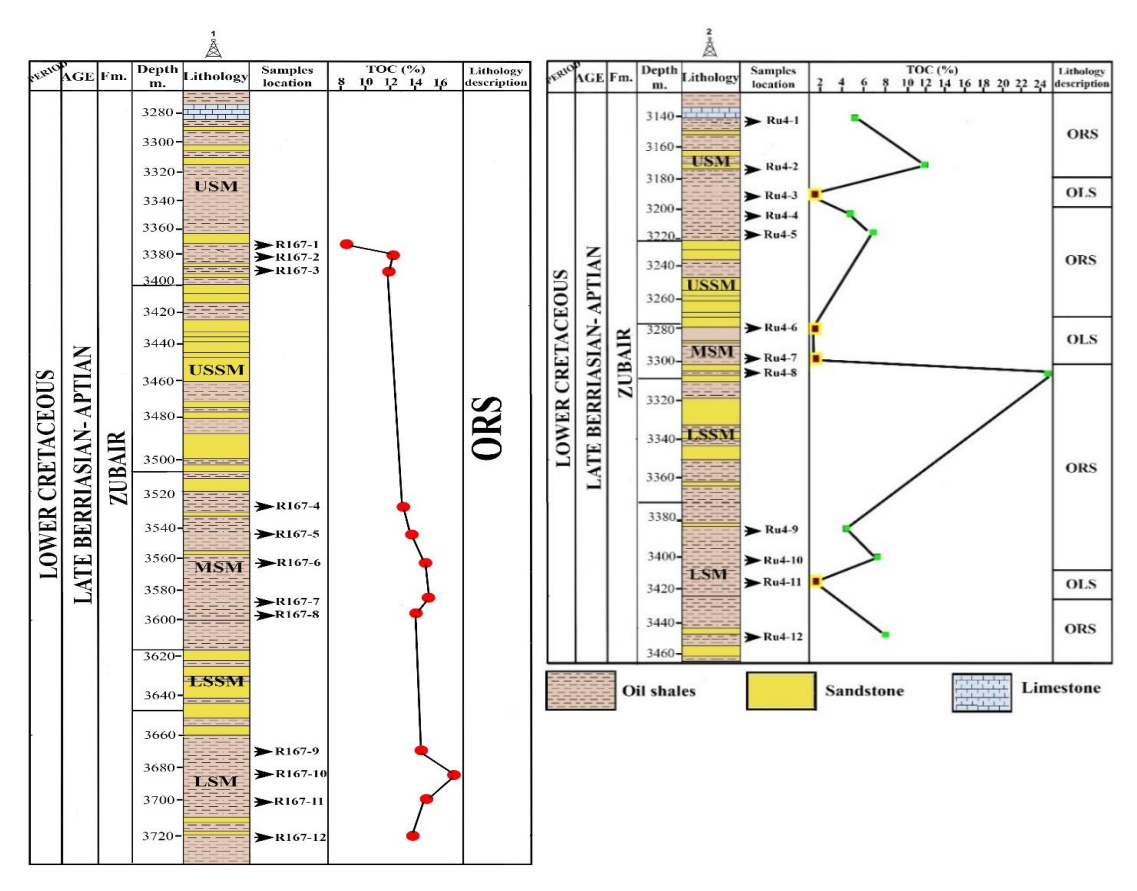


Fig. 2. Lithology and TOC values distributed vertically in the wells R167 and Ru4. The sample numbers are based on depth.

Major Oxides

The results of the major oxide analyses of the shales from wells R167 and Ru4 are shown in Tables 1 and 2, respectively. SiO_2 (detrital quartz and/or biogenic silica), Al_2O_3 (clay fraction), and CaO (carbonate material) are the three endmember oxides that can be combined to form marine shales (Xu et al., 2022). The most prevalent oxides in the ORS of R167 and Ru4, OLS of Ru4 samples are SiO_2 (average 60.83 and 62.57, 49.26%, respectively), afterwards Al_2O_3 (average 15.88 and 13.12, 21.95% respectively), and $T????Fe_2O_3$ (average 5.34 and 4.68, 6.61% respectively) (Tables 1 and 2). The ORS have a higher SiO_2 content than the OLS and a lower Al_2O_3 and Fe_2O_3 content.

The highest SiO₂ content and lowest Al₂O₃ content are found in the ORS. Al₂O₃ content increased significantly while SiO₂ content sharply declined in the OLS (Fig. 3). According to the statistics, Si, Al, Na, P, and Ti were moderately enriched ($1 \le EF \le 3$) for R167- ORS, while Si, Al, Ca, Mg, P, Ti, and Mn were moderately enriched for Ru4- ORS and only Al and Ti were moderately enriched for Ru4- OLS. Fe, Ca, Mg, K, and Mn were slightly depleted (EF < 1) in R167-ORS. Fe, Na, and K were slightly depleted in Ru4-ORS, while most elements are slightly depleted in Ru4-OLS except Al and Ti compared to the ORS (Fig. 4a).

Table 1: TOC and major components of oil shales in well R167, where EF represented by *= depletion, **= medium enrichment, ***= enrichment.

| Core No. | Lithology | Depth (m.) | TOC (%) | SiO ₂ (%) ** | $Al_2O_3(\%) **$ | $\mathrm{TFe_2O_3}\left(\%\right) *$ | CaO (%) * | ${ m MgO}\left(\% ight) *$ | Na ₂ O (%) ** | $ m K_2O~(\%)~*$ | $P_2O_5(\%) **$ | $\mathrm{TiO}_{2}\left(\%\right)**$ | MnO (%) * | Other (%) | $\mathrm{Fe}_2\mathrm{O}_3/\mathrm{TiO}_2$ | $Al_2O_3/(Al_2O_3 + Fe_2O_3)$ | Al/ (Al+ Fe+ Mn) |
|-------------|---------------------------|------------|---------|-------------------------|------------------|--------------------------------------|-----------|----------------------------|--------------------------|------------------|-----------------|-------------------------------------|-----------|-----------|--|-------------------------------|---------------------|
| | Upper Shale Member (USM) | | | | | | | | | | | | | | | | |
| R167-1 | =' | 3373 | 8.8 | 56.77 | 17.14 | 6.56 | 0.37 | 2.55 | 0.98 | 2.09 | 0.22 | 1.11 | 0.05 | 11.66 | 6.0 | 0.72 | 0.66 |
| R167-2 | _ | 3381 | 12.5 | 59.75 | 18.33 | 3.48 | 0.24 | 1.08 | 1.16 | 2.76 | 0.14 | 0.50 | 0.04 | 11.24 | 6.96 | 0.84 | 0.79 |
| R167-3 | _ | 3389 | 11.7 | 60.84 | 15.62 | 5.73 | 1.03 | 1.47 | 1.31 | 2.12 | 0.12 | 1.00 | 0.04 | 10.12 | 5.73 | 0.73 | 0.67 |
| | Middle Shale Member (MSM) | | | | | | | | | | | | | | | | |
| R167-4 | = | 3531 | 12.8 | 55.72 | 15.94 | 4.95 | 0.32 | 1.88 | 1.20 | 2.22 | 0.23 | 0.76 | 0.09 | 14.45 | 6.51 | 0.76 | 0.70 |
| R167-5 | | 3544 | 12.9 | 62.65 | 17.51 | 6.42 | 0.14 | 0.45 | 1.06 | 2.18 | 0.15 | 0.99 | 0.02 | 8.11 | 6.48 | 0.73 | 0.67 |
| R167-6 | ORS | 3563 | 13.7 | 55.62 | 14.72 | 5.64 | 2.55 | 2.71 | 0.95 | 2.59 | 0.24 | 0.92 | 0.07 | 13.14 | 6.13 | 0.72 | 0.65 |
| R167-7 | | 3577 | 15.5 | 61.88 | 13.55 | 5.37 | 1.77 | 2.19 | 1.10 | 1.47 | 0.13 | 1.04 | 0.03 | 11.20 | 5.16 | 0.71 | 0.65 |
| R167-8 | | 3590 | 14.5 | 62.84 | 16.23 | 4.34 | 0.71 | 1.42 | 1.00 | 2.15 | 0.27 | 0.85 | 0.03 | 9.12 | 5.10 | 0.79 | 0.73 |
| | _ | | | | | | Lower | Shale Mo | ember (I | LSM) | | | | | | | |
| R167-9 | _ | 3667 | 12.7 | 63.74 | 13.75 | 4.54 | 0.14 | 1.38 | 1.12 | 0.41 | 0.11 | 0.59 | 0.01 | 13.10 | 7.69 | 0.75 | 0.69 |
| R167-10 | _ | 3683 | 16.8 | 64.52 | 15.64 | 5.82 | 0.12 | 1.72 | 1.09 | 2.74 | 0.04 | 1.09 | 0.01 | 5.72 | 5.33 | 0.72 | 0.67 |
| R167-11 | _ | 3703 | 15.4 | 62.04 | 17.45 | 6.54 | 1.05 | 2.52 | 0.27 | 1.83 | 0.16 | 1.12 | 0.03 | 6.25 | 5.83 | 0.72 | 0.66 |
| R167-12 | | 3721 | 14.7 | 63.59 | 14.77 | 4.74 | 0.32 | 2.40 | 1.05 | 2.44 | 0.23 | 0.89 | 0.04 | 8.89 | 5.32 | 0.75 | 0.71 |

Table 2: TOC and major components of oil shales in well Ru4, where EF represented by *= depletion, **= medium enrichment, ***= enrichment.

| Core No. | Lithology | Depth (m.) | TOC (%) | SiO ₂ (%) | $\mathrm{Al}_2\mathrm{O}_3(\%)$ | $\mathrm{TFe_2O_3}\left(\%\right)$ | CaO (%) | MgO (%) | Na ₂ O (%) | K_2O (%) | P_2O_5 (%) | $TiO_2(\%)$ | MnO (%) | Other (%) | $\mathrm{Fe_2O_3/\ TiO_2}$ | $	ext{Al}_2	ext{O}_3/(ext{Al}_2	ext{O}_3+	ext{Fe}_2	ext{O}_3)$ | Al/ (Al+ Fe+ Mn) |
|-------------|--------------------------|------------|---------|----------------------|---------------------------------|------------------------------------|-----------|---------|-----------------------|------------|--------------|-------------|---------|-----------|----------------------------|---|------------------|
| | Upper Shale Member (USM) | | | | | | | | | | | | | | | | |
| Ru4-1 | ORS | 3145 | 5.7 | 67.23** | 13.29** | 5.25* | 1.02** | 1.75** | 0.54* | 1.95* | 0.14** | 0.99** | 0.17** | 7.22 | 5.30 | 0.71 | 0.64 |
| Ru4-2 | ō | 3175 | 11.8 | 65.72** | 12.22** | 3.17* | 0.13** | 2.55** | 1.07* | 2.74* | 0.11** | 0.58** | 0.15** | 10.12 | 5.46 | 0.79 | 0.72 |
| Ru4-3 | 0 L S | 3194 | 0.72 | 55.43* | 14.82** | 6.39* | 0.46* | 2.45* | 0.34* | 2.25* | 0.21* | 1.25** | 0.12* | 16.11 | 5.11 | 0.69 | 0.62 |
| Ru4-4 | ORS | 3203 | 4.5 | 66.56** | 12.27** | 5.04* | 0.11** | 2.56** | 0.01* | 1.41* | 0.10** | 0.95** | 0.08** | 9.87 | 5.30 | 0.70 | 0.64 |
| Ru4-5 | <u> </u> | 3218 | 6.7 | 64.33** | 12.38** | 3.27* | 0.77** | 1.51** | 0.47* | 2.54* | 0.02** | 0.62** | 0.14** | 12.34 | 5.27 | 0.79 | 0.72 |
| | | | | | | N | Iiddle Sh | ale Men | iber (MS | SM) | | | | | | | |
| Ru4-6 | STO | 3280 | 0.77 | 49.72* | 23.46** | 7.58* | 0.34* | 1.67* | 0.70* | 2.80* | 0.12* | 1.42** | 0.01* | 11.26 | 5.33 | 0.75 | 0.70 |
| Ru4-7 | <u> </u> | 3297 | 0.78 | 45.66* | 25.21** | 7.12* | 3.59* | 2.13* | 0.49* | 1.73* | 0.14* | 1.25** | 0.05* | 12.12 | 5.69 | 0.78 | 0.72 |
| Ru4-8 | 0 X S | 3309 | 25.5 | 68.34** | 12.63** | 3.25* | 3.95** | 3.17** | 0.73* | 1.52* | 0.04** | 0.57** | 0.18** | 6.22 | 5.70 | 0.79 | 0.72 |
| | | | | | | I | Lower Sh | ale Men | iber (LS | M) | | | | | | | |
| Ru4-9 | ORS | 3388 | 4.24 | 57.62** | 13.92** | 5.33* | 1.29** | 2.24** | 1.17* | 2.05* | 0.13** | 0.72** | 0.07** | 14.56 | 7.40 | 0.72 | 0.65 |
| Ru4-10 | Ō | 3408 | 5.7 | 54.74** | 13.65** | 5.52* | 1.92** | 1.98** | 1.05* | 3.54* | 0.22** | 1.02** | 0.11** | 15.77 | 5.41 | 0.71 | 0.64 |
| Ru4-11 | 0 L S | 3417 | 0.75 | 46.26* | 24.32** | 5.35* | 0.4* | 1.05* | 0.51* | 1.85* | 0.15* | 1.09** | 0.06* | 20.22 | 5.0 | 0.82 | 0.77 |
| Ru4-12 | 0 R S | 3447 | 7.6 | 56.06** | 14.66** | 6.66* | 3.48** | 2.41** | 0.39* | 2.05* | 0.23** | 1.00** | 0.12** | 12.52 | 6.66 | 0.68 | 0.61 |

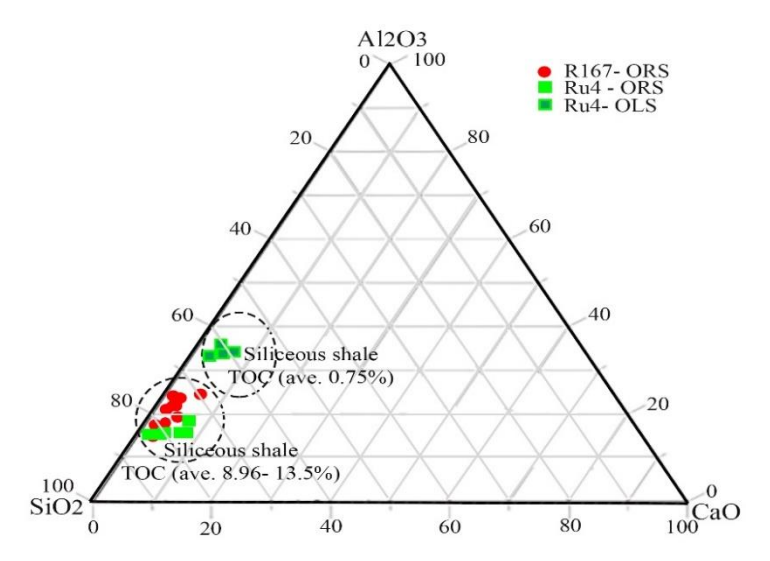


Fig. 3. SiO₂-Al₂O₃-CaO Ternary diagram of the contents of the ORS and OLS sections.

Trace Elements

Tables (3 and 4) display the findings of the trace element analysis. In ORS (R167 and Ru4), the EF values indicate that Zr and U are significantly enriched (EF > 3), Ni, Zn, and Hf are moderately enriched ($1 \le EF \le 3$), and V, Sc, Cr, Co, Cu, Rb, Sr, Ba, and Th are relatively depleted (EF < 1). According to EF values of OLS, Zr, Hf, and U are slightly enriched, while V, Sc, Cr, Co, Ni, Cu, Zn, Rb, Sr, Ba, and Th are relatively depleted. In comparison, the OLS contains less trace element content than the ORS (Fig. 4b).

Tables 5 and 6 show the findings of the REE analysis. The total REE contents (\sum REE) for R167 and Ru4- ORS range from 153.55 to 205.7 ppm (average 181.26 ppm), and 150.2 to 201.33 ppm (average 178.54 ppm) respectively. Due to the various lithologies, the \sum REE abundances of Ru4-OLS vary greatly, with average \sum REE abundances ranging from 164.94 to 192.57 ppm (mean 174.41 ppm). The ratios of \sum LREE/ \sum HREE and La_N/Yb_N can be used to determine the degree of differentiation of the REEs; more enriched light REE (LREE) contents are found when the values of these two parameters are higher (Fonseca et al., 2021). R167 and Ru4- ORS, and Ru4- OLS have \sum LREE/ \sum HREE ratios ranging from 7.09 to 10.99 (average 8.77), 6.27 to 11.83 (average 8.25), and 8.45 to 9.73 (average 9.00), respectively. The ratios of La_N/Yb_N of R167 and Ru4- ORS, and Ru4- OLS range from 0.42 to 1.22 (average 0.92), 0.48 to 1.74 (average 0.93), and 0.94 to 1.2 (average 1.05), respectively. Both \sum LREE/ \sum HREE and La_N/Yb_N ratios show that the OLS have much higher LREE contents. Different REE distribution curves can be seen in the ORS and OLS 's PAAS-normalized curves (Fig. 5).

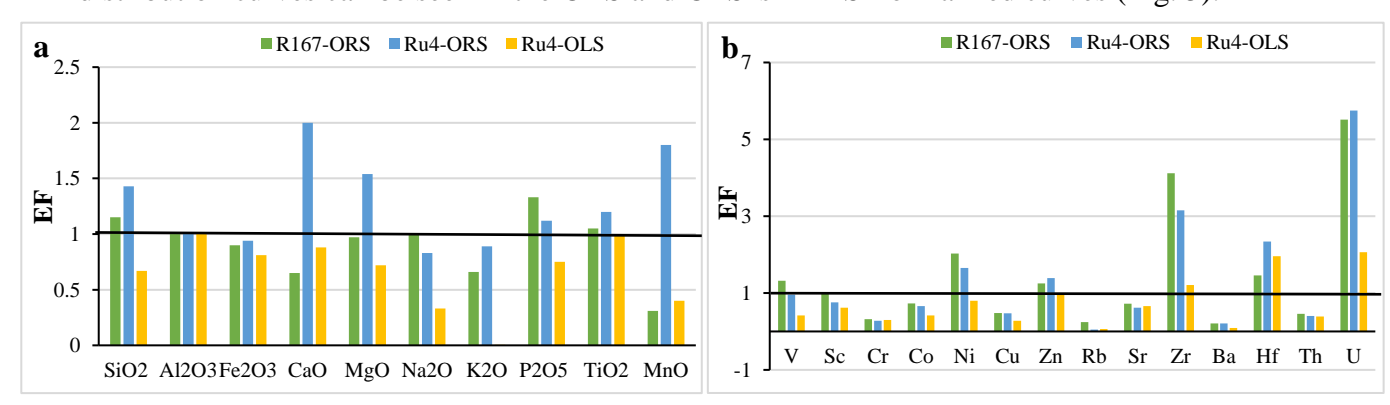


Fig. 4. (a) Major element EF values in relation to PAAS. (b) Trace element EF values in relation to PAAS. The elemental enrichment or depletion is indicated by EF=1 line.

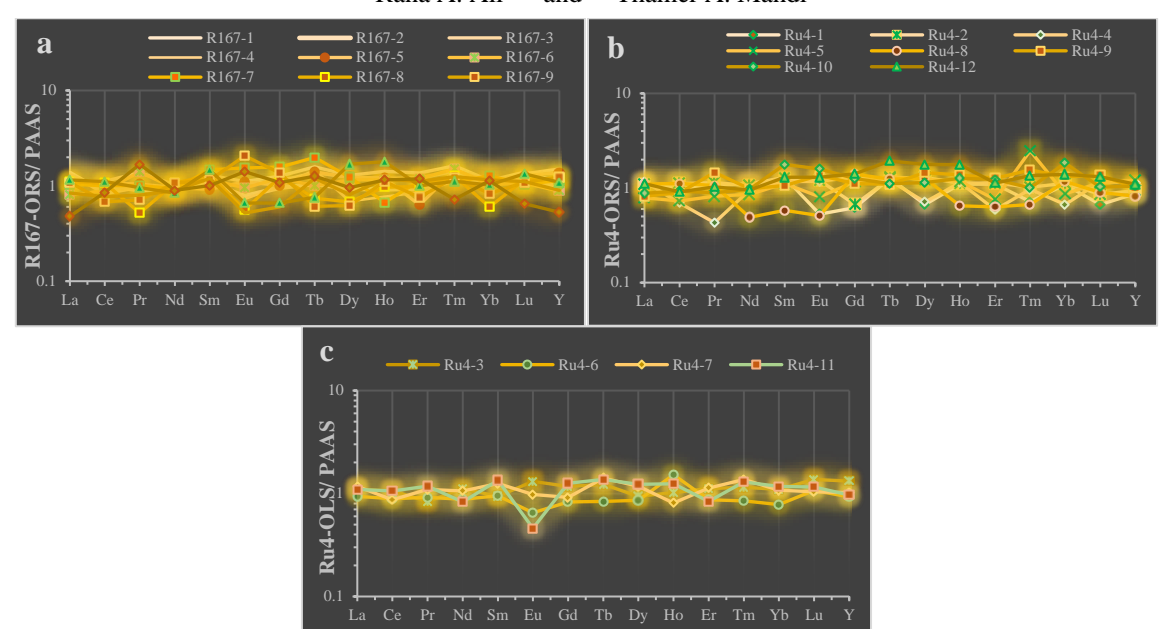


Fig. 5. (a) and (b) Patterns of PAAS-normalized REE distribution in samples from the R167 and Ru4-ORS, respectively. (c) Patterns of PAAS-normalized REE distribution in samples from the Ru4-OLS.

Table 3: Trace element content of the oil shales in the well R167, where EF represented by *= depletion, **= medium enrichment, ***=enrichment

| Core No. | R167- | R167- | R167- | R167- | R167- 5 | R167- | R167- | R167- 8 | R167- 9 | R167- 10 | R167- 11 | R167- 12 |
|--------------|--------|-------|-------|--------|------------|-------|-------|------------|------------|-------------|-------------|-------------|
| Depth (m.) | 3373 | 3381 | 3389 | 3531 | 3544 | 3563 | 3577 | 3590 | 3667 | 3683 | 3703 | 3721 |
| TOC (%) | 8.8 | 12.5 | 11.7 | 12.8 | 12.9 | 13.7 | 15.5 | 14.5 | 12.7 | 16.8 | 15.4 | 14.7 |
| V (ppm) ** | 145.0 | 224.0 | 197.1 | 67.3 | 170.2 | 233.0 | 95.6 | 175.5 | 194.0 | 180 | 79.6 | 234.8 |
| Sc (ppm) * | 10.70 | 9.10 | 16.0 | 12.5 | 15.0 | 10.8 | 16.0 | 16.0 | 11.10 | 14.0 | 14.4 | 15.0 |
| Cr (ppm) * | 30.0 | 35.0 | 33.89 | 11.2 | 31.0 | 35.9 | 20.0 | 27.4 | 31.5 | 34.5 | 17.3 | 50.8 |
| Co (ppm) * | 12.3 | 10.8 | 11.57 | 19.43 | 12.11 | 10.0 | 20.22 | 7.53 | 10.0 | 11.56 | 15.0 | 7.44 |
| Ni (ppm) ** | 117.25 | 88.9 | 95.03 | 100.55 | 90.7 | 70.9 | 121.7 | 90.0 | 77.5 | 114.53 | 108.2 | 55.09 |
| Cu (ppm) * | 15.15 | 16.6 | 27.5 | 23.3 | 20.4 | 25.7 | 16.8 | 18.2 | 17.33 | 20.32 | 20.54 | 19.7 |
| Zn (ppm) ** | 102.0 | 77.2 | 137.2 | 66.7 | 105.0 | 89.7 | 57.5 | 94.9 | 125.7 | 157.6 | 109.4 | 118.3 |
| Ga (ppm) | 21.7 | 9.3 | 17.4 | 22.3 | 19.7 | 16.4 | 21.11 | 16.7 | 15.17 | 11.15 | 13.24 | 14.25 |
| Rb (ppm) * | 50.7 | 47.2 | 42.5 | 60.7 | 24.8 | 65.5 | 19.9 | 17.4 | 15.7 | 11.2 | 14.8 | 23.3 |
| Sr (ppm) * | 110.4 | 145.2 | 121.8 | 150.0 | 137.3 | 158.5 | 139.2 | 123.4 | 133.0 | 97.7 | 163.0 | 92.0 |
| Zr (ppm) *** | 735.5 | 810.0 | 324.0 | 447.5 | 1220.2 | 380.0 | 309.3 | 430.0 | 640.0 | 1350.0 | 1110.0 | 970.0 |
| Ba (ppm) ** | 107.0 | 98.7 | 92.3 | 133.0 | 118.2 | 171.5 | 123.5 | 117.4 | 95.6 | 115.2 | 127.7 | 83.8 |
| Hf (ppm) ** | 5.38 | 7.82 | 6.85 | 5.11 | 7.57 | 5.05 | 7.32 | 7.57 | 2.59 | 5.94 | 5.51 | 6.97 |
| Th (ppm)* | 7.2 | 8.0 | 9.1 | 5.3 | 8.2 | 3.5 | 3.4 | 6.0 | 5.0 | 4.3 | 4.4 | 3.7 |
| U (ppm) *** | 15.2 | 14.29 | 15.07 | 13.19 | 12.35 | 9.7 | 14.14 | 15.55 | 17.27 | 19.24 | 14.05 | 12.27 |
| V/ Cr | 4.83 | 6.4 | 5.81 | 6.00 | 5.49 | 6.49 | 4.78 | 6.4 | 6.15 | 5.21 | 4.6 | 4.62 |
| Ni/ Co | 9.53 | 8.23 | 8.21 | 5.17 | 7.49 | 7.09 | 6.01 | 11.95 | 7.75 | 9.90 | 7.21 | 7.40 |
| U/ Th | 2.11 | 1.78 | 1.65 | 2.48 | 1.5 | 2.77 | 4.15 | 2.61 | 3.45 | 4.47 | 3.19 | 3.31 |
| Ni/ Al | 25.88 | 18.33 | 23.0 | 23.82 | 19.59 | 18.22 | 34.0 | 20.97 | 21.29 | 27.66 | 23.42 | 14.09 |
| Sr/ Cu | 7.28 | 8.74 | 4.42 | 6.43 | 6.73 | 6.16 | 8.28 | 6.78 | 7.67 | 4.8 | 7.93 | 3.65 |
| Sr/ Ba | 1.03 | 1.47 | 1.32 | 1.12 | 1.16 | 0.92 | 1.12 | 1.05 | 1.39 | 0.84 | 1.27 | 1.09 |
| Th/ Sc | 0.67 | 0.87 | 0.56 | 0.42 | 0.54 | 0.32 | 0.21 | 0.37 | 0.45 | 0.30 | 0.30 | 0.24 |
| Zr/ Sc | 68.73 | 89.01 | 20.25 | 35.8 | 81.34 | 35.18 | 19.33 | 26.87 | 57.65 | 96.42 | 77.08 | 64.66 |
| Rb/ Sr | 0.46 | 0.32 | 0.34 | 0.4 | 0.18 | 0.41 | 0.14 | 0.14 | 0.11 | 0.11 | 0.09 | 0.25 |

Table 4: Trace element content of the oil shales in the well Ru4, where EF represented by *= depletion, **= medium enrichment, ***=enrichment; black color ORS and underlined red color OLS

| Core No. | Ru4-1 | Ru4-2 | <u>Ru4-3</u> | Ru4-4 | Ru4-5 | <u>Ru4-6</u> | <u>Ru4-7</u> | Ru4-8 | Ru4-9 | Ru4- 10 | <u>Ru4-</u> <u>11</u> | Ru4- 12 |
|------------|--------|---------|--------------|---------|---------|--------------|--------------|--------|--------|------------|--------------------------|------------|
| Depth (m.) | 3145 | 3175 | 3194 | 3203 | 3218 | 3280 | 3297 | 3309 | 3388 | 3408 | 3417 | 3447 |
| TOC (%) | 5.7 | 11.8 | 0.72 | 4.5 | 6.7 | 0.77 | 0.78 | 25.5 | 4.24 | 5.7 | 0.75 | 7.6 |
| V (ppm) | 133.0* | 92.2* | 35.7* | 72.5* | 127.6* | 55.5* | 63.33* | 134.0* | 77.4* | 97.07* | 141.0* | 65.72* |
| Sc (ppm) | 3.0* | 10.10* | 10.8* | 4.0* | 12.0* | 14.0* | 8.0* | 2.0* | 14.5* | 9.8* | 12.9* | 12.5* |
| Cr (ppm) | 22.21* | 31.2* | 13.5* | 23.28* | 19.54* | 25.5* | 35.7* | 22.21* | 10.0* | 34.4* | 79.6* | 11.5* |
| Co (ppm) | 7.38* | 11.45* | 14.5* | 9.45* | 6.29* | 8.21* | 7.97* | 7.47* | 11.13* | 13.0* | 8.5* | 8.09* |
| Ni (ppm) | 61.0** | 83.55** | 76.54* | 67.74** | 65.65** | 48.81* | 40.92* | 47.7** | 71.0** | 50.25** | 40.42* | 57.24** |

| Cu (ppm) | 6.41* | 8.21* | 11.92* | 7.34* | 31.2* | 14.8* | 20.3* | 9.33* | 19.86* | 23.39* | 18.21* | 26.6* |
|----------|---------|---------|--------|---------|---------|--------|--------|---------|--------|---------|---------|---------|
| Zn (ppm) | 138.5** | 157.7** | 44.5* | 147.4** | 94.05** | 87.9* | 42.2* | 82.15** | 36.6** | 109.5** | 39.7* | 101.2** |
| Ga (ppm) | 12.67 | 11.15 | 13.46 | 15.65 | 12.89 | 12.58 | 14.9 | 16.5 | 14.24 | 13.2 | 8.25 | 11.07 |
| Rb (ppm) | 2.49* | 4.0* | 12.2* | 3.31* | 5.2* | 21.7* | 9.2* | 1.0* | 11.4* | 13.6* | 7.7* | 10.2* |
| Sr (ppm) | 47.4* | 56.6* | 137.2* | 148.8* | 60.8* | 150.3* | 170.3* | 38.8* | 109.9* | 118.6* | 163.5* | 112.7* |
| Zr (ppm) | 333.2** | 345.3* | 270.7* | 537.5** | 422.0** | 372.3* | 170.5* | 1027.2 | 233.0* | 387.8** | 373.5** | 390.0* |
| Ba (ppm) | 35.5* | 49.7* | 30.0* | 106.3* | 119.0* | 39.8* | 40.4* | 63.3* | 127.7* | 143.2* | 170.3* | 122.8* |
| Hf (ppm) | 6.15** | 6.07** | 4.53** | 5.95** | 7.47** | 4.17** | 3.58** | 15.3** | 5.79** | 6.30** | 5.36** | 4.37** |
| Th (ppm) | 7.3* | 6.3* | 7.8* | 4.7* | 5.8* | 8.7* | 8.3* | 4.9* | 4.6* | 4.52* | 6.2* | 4.4* |
| U (ppm) | 17.8*** | 16.25* | 8.63** | 14.26** | 9.44*** | 7.9** | 7.19** | 15.45* | 8.41** | 7.6*** | 5.22** | 7.95** |
| V/ Cr | 5.98 | 2.95 | 2.64 | 3.11 | 6.53 | 2.17 | 1.77 | 6.03 | 7.74 | 2.82 | 1.77 | 5.71 |
| Ni/ Co | 8.26 | 7.29 | 5.27 | 7.16 | 10.43 | 5.94 | 5.13 | 6.38 | 6.37 | 3.86 | 4.75 | 7.07 |
| U/ Th | 2.43 | 2.58 | 1.10 | 3.03 | 1.62 | 0.90 | 0.82 | 3.15 | 1.82 | 1.68 | 0.84 | 1.80 |
| Ni/ Al | 17.37 | 25.86 | 19.52 | 20.90 | 20.07 | 7.86 | 6.13 | 14.28 | 19.29 | 13.92 | 6.28 | 14.75 |
| Sr/ Cu | 7.39 | 6.89 | 11.51 | 6.88 | 1.94 | 10.15 | 8.39 | 4.15 | 5.53 | 5.07 | 8.97 | 4.23 |
| Sr/ Ba | 1.33 | 1.13 | 4.57 | 1.39 | 0.51 | 3.77 | 4.21 | 0.61 | 0.86 | 0.82 | 0.96 | 0.91 |
| Th/ Sc | 2.43 | 0.62 | 0.72 | 1.17 | 0.48 | 0.62 | 1.03 | 2.45 | 0.31 | 0.46 | 0.48 | 0.35 |
| Zr/Sc | 111.06 | 34.18 | 25.06 | 134.37 | 35.16 | 26.59 | 21.31 | 513.6 | 16.06 | 39.57 | 28.95 | 31.2 |
| Rb/ Sr | 0.05 | 0.07 | 0.14 | 0.02 | 0.08 | 0.14 | 0.05 | 0.02 | 0.1 | 0.11 | 0.04 | 0.09 |
| | | | | | | | | | | | | |

Table 5: Oil shale REE contents in well R167.

| Core No. | R167-1 | R167-2 | R167-3 | R167-4 | R167-5 | R167-6 | R167-7 | R167-8 | R167-9 | R167- 10 | R167- 11 | R167- 12 |
|-----------------------------------|--------|--------|--------|--------|--------|--------|--------|--------|--------|-------------|-------------|-------------|
| La (ppm) | 42.25 | 52.00 | 43.51 | 50.55 | 40.90 | 30.44 | 39.70 | 42.42 | 41.72 | 32.18 | 43.99 | 18.55 |
| Ce (ppm) | 71.93 | 67.76 | 89.72 | 72.84 | 86.28 | 71.13 | 80.58 | 85.92 | 54.55 | 62.22 | 89.28 | 68.46 |
| Pr (ppm) | 8.00 | 8.73 | 12.2 | 8.20 | 9.40 | 12.47 | 9.04 | 4.70 | 6.33 | 7.17 | 8.60 | 14.98 |
| Nd (ppm) | 30.23 | 31.22 | 32.96 | 29.30 | 30.46 | 30.15 | 29.98 | 34.40 | 34.24 | 28.70 | 27.15 | 28.80 |
| Sm (ppm) | 7.27 | 5.95 | 5.44 | 7.22 | 5.17 | 6.51 | 8.25 | 7.27 | 6.45 | 6.74 | 8.18 | 5.70 |
| Eu (ppm) | 1.23 | 0.86 | 1.17 | 0.81 | 1.21 | 1.05 | 1.70 | 0.62 | 2.27 | 0.58 | 0.73 | 1.56 |
| Gd (ppm) | 5.94 | 4.52 | 5.31 | 4.66 | 4.75 | 5.72 | 7.42 | 5.85 | 6.43 | 2.85 | 3.12 | 5.10 |
| Tb (ppm) | 1.22 | 0.81 | 1.06 | 1.13 | 1.08 | 0.77 | 1.53 | 0.57 | 0.47 | 0.93 | 0.59 | 0.97 |
| Dy (ppm) | 5.69 | 4.09 | 5.45 | 3.06 | 5.44 | 5.07 | 5.42 | 3.00 | 2.74 | 3.57 | 7.47 | 4.25 |
| Ho (ppm) | 1.42 | 0.92 | 1.20 | 0.77 | 1.21 | 1.15 | 0.67 | 0.97 | 1.11 | 1.18 | 1.79 | 1.15 |
| Er (ppm) | 3.95 | 2.72 | 3.51 | 2.50 | 1.85 | 3.47 | 3.29 | 2.85 | 2.21 | 3.23 | 2.91 | 3.42 |
| Tm (ppm) | 0.65 | 0.47 | 0.57 | 0.45 | 0.58 | 0.60 | 0.44 | 0.51 | 0.49 | 0.50 | 0.45 | 0.29 |
| Yb (ppm) | 3.21 | 3.13 | 3.02 | 3.34 | 3.12 | 2.89 | 3.57 | 4.69 | 2.35 | 3.22 | 2.87 | 3.18 |
| Lu (ppm) | 0.6 | 0.49 | 0.58 | 0.46 | 0.55 | 0.46 | 0.45 | 0.50 | 0.47 | 0.48 | 0.58 | 0.28 |
| Y (ppm) | 29.70 | 25.90 | 40.50 | 27.82 | 37.20 | 23.80 | 30.80 | 32.72 | 33.32 | 24.5 | 29.6 | 24.55 |
| ∑REE (ppm) | 183.59 | 183.67 | 205.7 | 185.29 | 192.00 | 171.88 | 192.04 | 191.27 | 161.83 | 153.55 | 197.71 | 156.69 |
| LREE (ppm) | 160.91 | 166.52 | 185.00 | 168.92 | 173.42 | 151.75 | 169.25 | 175.33 | 145.56 | 137.59 | 177.93 | 138.05 |
| HREE (ppm) | 22.68 | 17.15 | 20.70 | 16.37 | 18.58 | 20.13 | 22.79 | 15.94 | 16.27 | 15.93 | 19.78 | 18.64 |
| LREE/ HREE | 7.09 | 9.70 | 8.93 | 10.31 | 9.33 | 7.53 | 7.42 | 10.99 | 8.94 | 8.63 | 8.99 | 7.40 |
| La _N / Yb _N | 0.97 | 1.22 | 1.06 | 1.11 | 0.96 | 0.77 | 0.81 | 0.66 | 1.31 | 0.73 | 1.12 | 0.42 |
| La/ Th | 5.86 | 6.50 | 4.78 | 9.53 | 4.98 | 8.69 | 11.67 | 7.07 | 8.34 | 7.48 | 10.00 | 5.01 |
| La _N / Ce _N | 1.24 | 1.62 | 1.01 | 1.46 | 1.00 | 0.89 | 1.04 | 1.03 | 1.60 | 1.09 | 1.03 | 0.56 |
| Eu/ Sm | 0.17 | 0.14 | 0.21 | 0.11 | 0.23 | 0.16 | 0.20 | 0.08 | 0.35 | 0.08 | 0.09 | 0.27 |
| Sm/ Yb | 2.26 | 1.90 | 1.80 | 2.16 | 1.65 | 2.25 | 2.31 | 4.30 | 2.74 | 2.09 | 2.85 | 1.79 |
| Y/Ho | 20.91 | 28.15 | 33.75 | 36.12 | 30.74 | 20.69 | 45.97 | 33.73 | 30.01 | 20.76 | 16.53 | 21.34 |
| La _n / Yb _n | 8.94 | 11.28 | 9.79 | 10.28 | 8.91 | 7.15 | 7.55 | 6.14 | 12.06 | 6.79 | 10.41 | 3.96 |
| δ Се | 0.89 | 0.71 | 0.89 | 0.81 | 1.01 | 0.81 | 0.98 | 1.32 | 0.75 | 0.94 | 1.05 | 0.78 |

Table 6: Oil shale REE contents in well Ru4.

| Core No. | Ru4-1 | Ru4-2 | Ru4-3 | Ru4-4 | Ru4-5 | Ru4-6 | Ru4-7 | Ru4-8 | Ru4-9 | Ru4- 10 | Ru4- 11 | Ru4- 12 |
|------------|--------|--------|--------|--------|--------|--------|--------|--------|--------|------------|------------|------------|
| La (ppm) | 42.05 | 41.72 | 35.22 | 44.66 | 30.20 | 35.77 | 44.72 | 42.05 | 31.27 | 33.74 | 41.95 | 42.45 |
| Ce (ppm) | 79.52 | 88.72 | 85.45 | 55.70 | 58.75 | 80.17 | 76.62 | 90.08 | 71.25 | 74.74 | 84.91 | 72.90 |
| Pr (ppm) | 9.45 | 10.16 | 7.50 | 3.85 | 7.33 | 8.19 | 9.83 | 9.49 | 13.02 | 8.00 | 10.52 | 9.20 |
| Nd (ppm) | 35.52 | 34.0 | 35.50 | 30.40 | 27.50 | 28.38 | 34.20 | 15.74 | 31.43 | 31.30 | 26.73 | 30.39 |
| Sm (ppm) | 7.24 | 7.21 | 5.27 | 6.51 | 6.24 | 5.33 | 7.02 | 3.25 | 5.94 | 9.95 | 7.55 | 7.28 |
| Eu (ppm) | 0.59 | 1.32 | 1.45 | 1.30 | 0.90 | 0.72 | 1.08 | 0.57 | 1.50 | 1.75 | 0.51 | 1.43 |
| Gd (ppm) | 2.91 | 3.18 | 5.52 | 6.12 | 5.49 | 3.90 | 4.32 | 6.60 | 5.24 | 5.92 | 5.94 | 6.66 |
| Tb (ppm) | 0.98 | 0.97 | 0.95 | 0.93 | 1.02 | 0.65 | 1.09 | 0.96 | 0.85 | 0.86 | 1.06 | 1.49 |
| Dy (ppm) | 2.95 | 5.70 | 4.17 | 3.12 | 5.44 | 3.78 | 5.22 | 5.59 | 6.39 | 5.02 | 5.42 | 7.84 |
| Ho (ppm) | 1.10 | 1.13 | 1.02 | 1.14 | 1.18 | 1.52 | 0.81 | 0.65 | 1.38 | 1.27 | 1.24 | 1.30 |
| Er (ppm) | 3.17 | 3.29 | 3.27 | 1.73 | 2.22 | 2.53 | 3.29 | 1.83 | 3.70 | 3.57 | 2.44 | 3.29 |
| Tm (ppm) | 0.29 | 0.41 | 0.46 | 0.39 | 0.99 | 0.34 | 0.55 | 0.27 | 0.62 | 0.40 | 0.52 | 0.54 |
| Yb (ppm) | 3.04 | 3.15 | 3.10 | 1.90 | 2.45 | 2.20 | 3.03 | 3.30 | 3.71 | 5.13 | 3.28 | 3.93 |
| Lu (ppm) | 0.29 | 0.37 | 0.59 | 0.50 | 0.49 | 0.46 | 0.45 | 0.39 | 0.59 | 0.44 | 0.50 | 0.57 |
| Y (ppm) | 23.70 | 25.55 | 35.70 | 30.91 | 32.70 | 25.20 | 27.70 | 22.30 | 27.20 | 28.40 | 26.40 | 29.70 |
| ∑REE (ppm) | 189.1 | 201.33 | 189.47 | 158.25 | 150.2 | 164.94 | 185.23 | 180.77 | 176.89 | 182.09 | 192.57 | 189.73 |
| LREE (ppm) | 174.37 | 183.13 | 170.39 | 142.42 | 130.92 | 149.56 | 166.47 | 161.18 | 154.41 | 159.48 | 172.17 | 163.65 |
| HREE (ppm) | 14.73 | 18.20 | 19.08 | 15.83 | 19.28 | 15.38 | 18.76 | 19.59 | 22.48 | 22.61 | 20.40 | 26.08 |

0.85

| | | | K | ana A. An | and | 1 Haiii | er A. Ma | ınaı | | | | 333 |
|----------------------|---------------------|-------|-------|-----------|-------|---------|----------|-------|-------|-------|-------|-------|
| LREE/ HI | REE 11.83 | 10.06 | 8.93 | 8.99 | 6.79 | 9.73 | 8.87 | 8.22 | 6.86 | 7.05 | 8.45 | 6.27 |
| La _N / Yt | o _N 1.01 | 0.97 | 1.00 | 1.74 | 0.90 | 1.20 | 1.08 | 0.94 | 0.62 | 0.48 | 0.94 | 0.79 |
| La/ Th | 5.76 | 6.62 | 4.51 | 9.50 | 11.18 | 4.11 | 5.38 | 8.58 | 6.79 | 7.46 | 6.76 | 9.64 |
| La _N / Ce | e _N 1.11 | 0.98 | 1.03 | 1.69 | 1.08 | 1.05 | 1.34 | 0.98 | 0.92 | 0.94 | 1.03 | 1.22 |
| Eu/ Sn | n 0.08 | 0.18 | 0.27 | 0.19 | 0.14 | 0.13 | 0.15 | 0.17 | 0.25 | 0.17 | 0.06 | 0.19 |
| Sm/ Yl | b 2.38 | 2.28 | 1.70 | 3.42 | 2.54 | 2.42 | 2.31 | 0.98 | 1.60 | 1.93 | 2.30 | 1.85 |
| Y/Ho | 21.54 | 22.61 | 35.00 | 27.11 | 27.71 | 16.57 | 34.19 | 34.30 | 19.71 | 22.36 | 21.29 | 22.84 |
| La _n / Yb | o _n 9.39 | 9.00 | 7.72 | 15.96 | 8.37 | 11.04 | 10.02 | 8.65 | 5.72 | 4.46 | 8.69 | 7.33 |

Thomas A Mahdi

0.84

1.03

0.78

1.05

0.92

Discussion

Provenance, recycling, and tectonic setting

1.09

0.86

Some immobile elements, including Sc, Th, La, Zr, and Hf, can be transferred from the provenance area and still retain the traces of the source area. Moreover, following sedimentary recycling into clastic rocks, Zr is readily enriched (Wu et al., 2021; Fathy et al., 2021). The levels of sedimentary recycling of the parent rock are indicated by bivariate plots of Zr/Sc vs. Th/Sc (Wu et al., 2021; Janssen et al., 2023). The findings in this study demonstrate that felsic parent rock composition controls the composition of oil shales, and sedimentary recycling has little to no impact on any of the samples (Ali, 2023; Ali and Jassim, 2023). The bivariate plots of Hf vs. La/Th are widely employed to denote parent rock types because certain trace elements, like Hf, Th, and La, are comparatively stable throughout deposition and diagenesis (Mahmoud et al., 2023). The findings also demonstrated that a mixture of felsic and intermediate rocks served as the primary material source for the parent rock in oil shales (Fig. 6a, b). Diagenesisstable major and REEs like Ti, Fe, Al, Ce, and La can be used to determine the parent rocks' sedimentary environment. Sedimentary rocks' tectonic environment is determined by variables like Fe₂O₃/TiO₂, Al₂O₃/(Al₂O₃+Fe₂O₃), and La_N/Ce_N (the subscript N denotes PAASnormalization). The majority of the samples are scattered along the continental margin, according to the bivariate graphs of Fe₂O₃/TiO₂- Al₂O₃/ (Al₂O₃+ Fe₂O₃) and La_N/Ce_N- Al₂O₃/ $(Al_2O_3 + Fe_2O_3)$ (Fig. 6c, d).

Paleoenvironment

1. Silica Origin and Terrigenous Input

According to earlier research, the four primary sources of silica in sedimentary rocks are pyroclastic rocks, terrigenous clastics, hydrothermal fluids, and siliceous organisms (Liao et al., 2018). Siliceous rocks with and without hydrothermal activity can be distinguished by the Al- Fe- Mn ternary diagram (Ma et al., 2019). The results demonstrate that silica in both the ORS and the OLS had a non-hydrothermal origin (Fig. 7a). Hydrothermal activity is also assessed using the REE ratios, including Sm/ Yb, Eu/ Sm, and Y/ Ho. Accordingly, the samples found in oil shales are close to seawater and hydrogenetic Fe-Mn crusts, suggesting that less than 0.1% of the seafloor is thermally active (Fig. 7b, c). For the OLS, there is a positive correlation between the contents of SiO₂ and Al₂O₃, suggesting that the silica primarily originates from terrigenous clastics. For the ORS, there is no clear correlation between the contents of SiO₂ and Al₂O₃, suggesting the existence of non-terrigenous silica (Fig. 7d). The non-hydrothermal nature of each sample indicates that some of the silica found in ORS comes from siliceous organisms (Fang et al., 2023). The biogenic silica content (Si_{xs}) in the ORS R167, Ru4, and OLS Ru4 ranges from 21.56 to 25.01% (average 23.58%), 21.23 to 26.48% (average 24.26%), and 17.73 to 21.49% (average 19.11%), respectively, based on formula (2) above. This revealed that the ORS contained significantly more Si_{xs} than the OLS (Fig. 8). Si_{xs} content in Ru4 is abruptly dropped from 25.48% in sample Ru4-2 to 21.49% in sample Ru4-3. And Sr/Cu and Sr/Ba both experienced a sudden increase from 6.89 to 11.51 and 1.13 to 4.57, respectively. Also increase from 24.94% of sample Ru4-5 to 19.29 and 17.73% for samples Ru4-6 and 7, respectively. Sr/Cu and Sr/Ba ratios for Ru4-5 unexpectedly jumped from 1.94 and 0.51 to 10.15 and 3.77 for Ru4-6, and to 8.39 and 4.21 for Ru4-7, respectively. This Si_{xs} decrease and Sr/Cu, Sr/Ba increase also occurred in the lower part of well Ru-4, suggesting the paleo-salinity and paleo-climate impact on Si_{xs} content (Wu et al., 2021). As the sea level dropped, a warm, humid climate, higher salinity of seawater, and weaker nutrients, the upwelling in the deep shelf all combined to cause a bigger water mass restriction, and a sharp decline in microorganisms, which resulted in a sharp decline in the content of Si_{xs}.

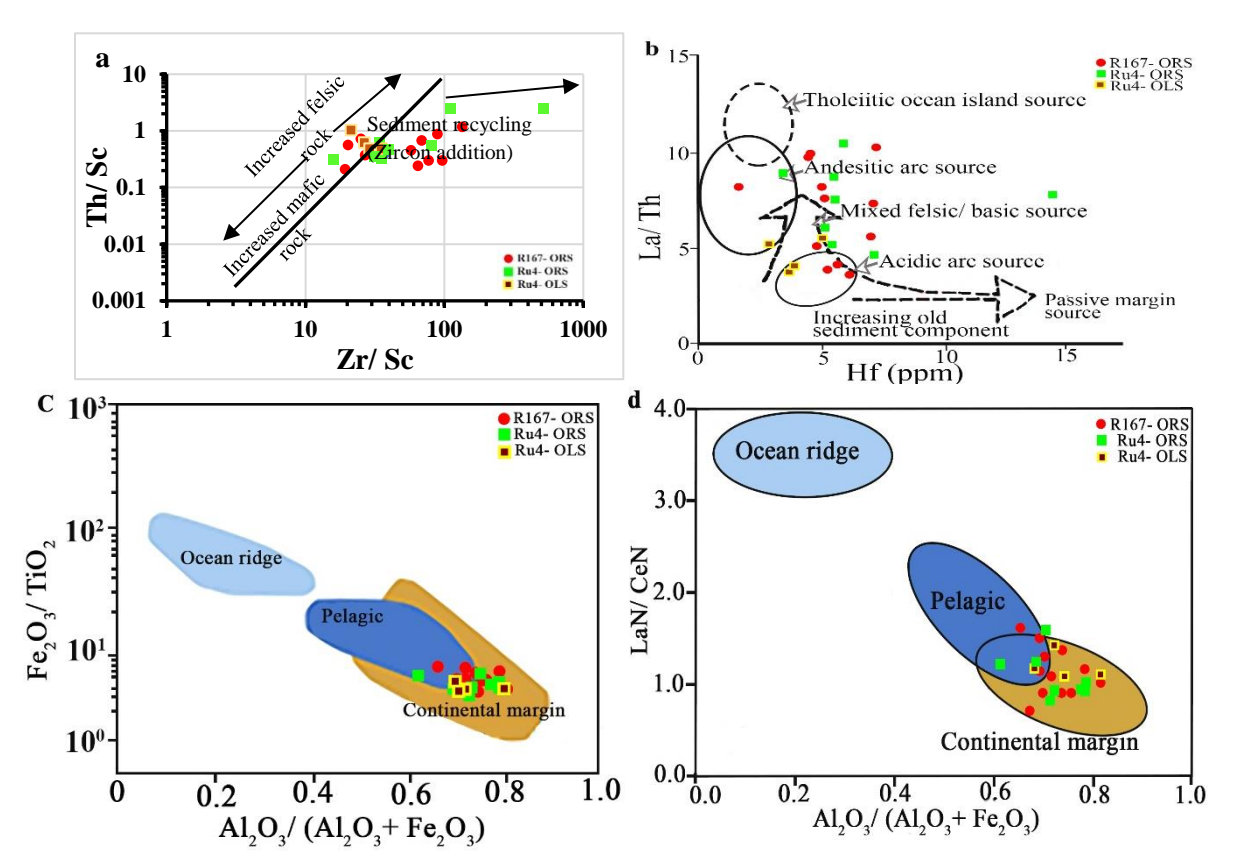


Fig. 6. Cross-plots of the ORS and OLS for the oil shales for (a) Th/Sc vs. Zr/Sc. (b) La/Th vs. Hf. (c) Fe₂O₃/TiO₂ vs. Al₂O₃/(Al₂O₃+ Fe₂O₃). (d) La_N/Ce_N vs. Al₂O₃/(Al₂O₃+ Fe₂O₃).

The results indicate that high biogenic silica content or low terrestrial siliciclastic inputs in marine oil shale do not necessarily produce significantly rich organic matter. Here, rather than an evident linear relationship, a complex interaction exists between silica of varied origin and the accumulation of organic matter. In the study of the terrestrial inputs, the elements Ti, Al, Zr, and Th are frequently used (Zeng et al., 2015; Wang et al., 2017). Al and Ti concentrations in shale samples gradually increased in Ru4-OLS compared to Ru4 and R167-ORS, with average concentrations of 4.20 and 0.54%, 3.47 and 0.49%, and 5.80 and 0.75% for the R167, Ru4-ORS, and Ru4-OLS, respectively (Table 1, Table 2, and Fig. 8). One of the likely causes of the gradual decline in the Si_{xs} content is the reduction of organic matter within sediments caused by the increase in the terrigenous input in some samples of Ru4 (Fig. 8).

However, the contents of Al and Ti increase slightly from Ru4-2 to Ru4-3, Ru4-5 to Ru4-6, and Ru4-7, Ru4-10 to Ru4-11. In contrast, the contents of Si_{xs} decrease significantly (Fig. 8), indicating that the increasing Al and Ti contents are not the primary factor that caused a sharp decrease in the Si_{xs} content.

2. Paleoredox Conditions

Paleo-redox conditions in oil shales of R167 and Ru4 have been studied using the prevalent proxies of V/Cr, Ni/Co, U/Th, and δ Ce mentioned above (Xu et al., 2022; Liu et al., 2023). The alteration in redox conditions has gone through at least three stages, from euxinic to anoxic to suboxic, according to a thorough comparison of the indicators of V/Cr, Ni/Co, U/Th, and δ Ce (Fig. 9).

Stage I consists of the entire ORS - R167 (R167-1 - R167-12), as well as the upper, middle, and lower ORS - Ru4 (Ru4-1, Ru4-4, Ru4-5, Ru4-8, Ru4-9, and Ru4-12), with

average V/Cr, Ni/Co, U/Th, and δCe ratios of 5.56, 8.00, 3.25, and 0.91 for well R167, respectively. And 5.85, 7.61, 2.30, and 0.89 for well Ru4, showing that the paleo-ocean experienced *euxinic* conditions.

Stage II is the upper, middle, and lower parts of the ORS - Ru4 (Ru4-2, Ru4-7, and Ru4-11), with V/Cr, Ni/Co, U/Th, and δCe ratios of 2.16, 5.72, 1.41, and 0.92, respectively, showing *anoxic to suboxic* conditions within the paleo-ocean.

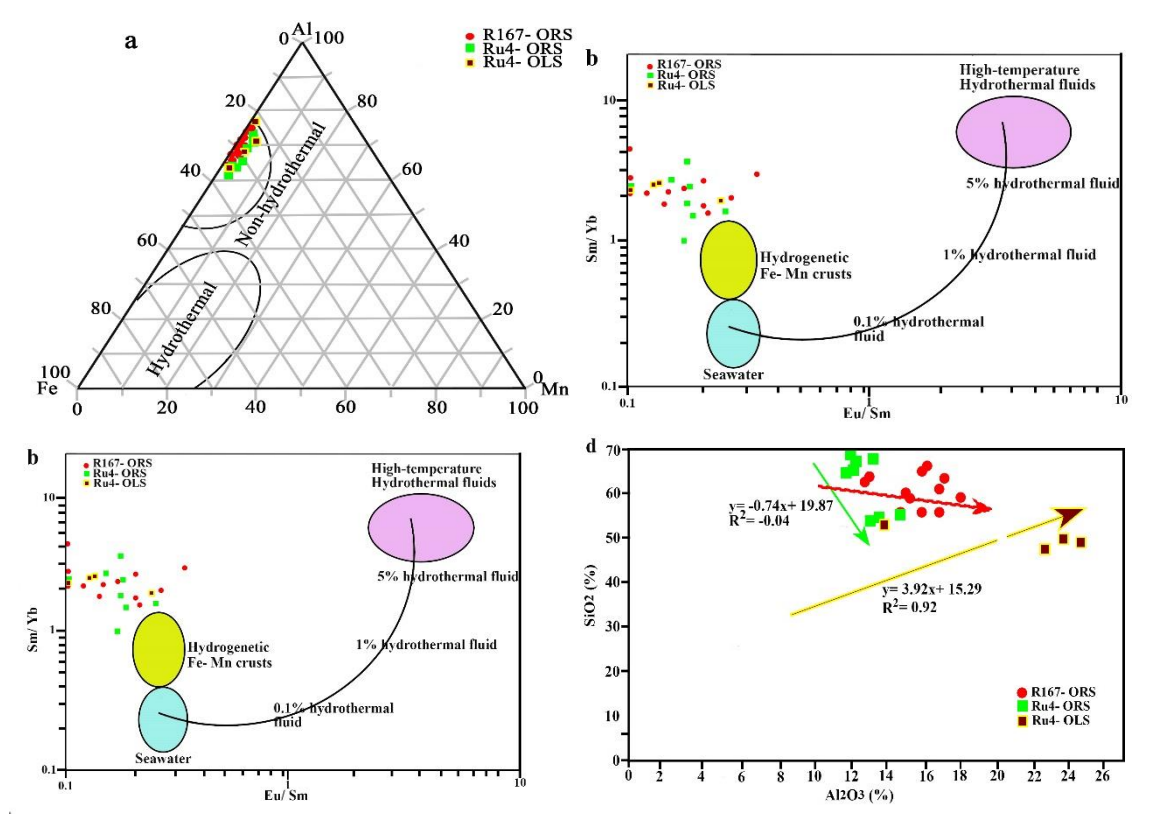


Fig. 7. (a) Al- Fe- Mn ternary graph showing the hydrothermal origin of the ORS and the OLS. (b) Sm/Yb vs. Eu/Sm cross-plots showing the hydrothermal origin of the ORS and the OLS. (c) Y/ Ho vs. Eu/ Sm cross-plots: a, b, and c to pinpoint the Zubair oil shales' hydrothermal origins for the ORS and the OLS. (d) A correlation between the SiO₂ and Al₂O₃ content of the ORS and OLS in Zubair oil shales.

Stage III is the OLS-Ru4 (Ru4-3, Ru4-6, and Ru4-10), with average ratios of V/Cr, Ni/Co, U/Th, and δ Ce of 2.54, 5.02, 1.22, and 1.07, respectively, showing *suboxic to oxic* conditions within the paleo-ocean.

The data from well RU4 show that the deposition transitioned from euxinic to anoxic to suboxic conditions from the lower to the upper section. The study findings are in line with those of Idan et al. (2019), which show that all of the R167-ORS and the upper, middle, and lower parts of the Ru4-ORS were euxinic and anoxic before gradually changing to suboxic (OLS). A restricted hydrodynamic environment with H₂S tends to enrich the trace element Mo (Algeo et al., 2009; Li et al., 2017). Typically, a sedimentary fluid body's paleoenvironment and cycle of water conditions are deduced using the UEF and MoEF covariant model.

The Mo_{EF}/U_{EF} ratios are stable at a range of about 1-3 times the amount of sea water with an increase in the Mo_{EF} and U_{EF} values, showing that the paleo-ocean had been semi-stagnant and semi-closed (Fig. 10a). The Mo/TOC ratios for the ORS in wells R167 and Ru4 vary between 9.43×10^{-4} - 60.27×10^{-4} (average 25.52×10^{-4}), and 7.79×10^{-4} - 58.72×10^{-4} (average 23.64×10^{-4}) respectively, indicating that the ORS were primarily generated in a semi-stagnant to strongly stagnant environment. The OLS Mo/TOC ratios range from 2.97×10^{-4} - 19.52×10^{-4} (average 12.51×10^{-4}), suggesting that the OLS also primarily formed in a semi-stagnant to strongly stagnant environment (Fig. 10b). It is notable that the OLS 's level of stagnation is marginally higher. Ma et al. (2019) revealed that the Mo/TOC ratios of the

ORS and OLS are almost as low as those of the strongly restricted Black Sea basin but still slightly higher than those of the modern Framvaren Fjord and Cariaco basins. This suggests that western Hubei is relatively connected to the open ocean, and in this environment, the upwelling of nutrients is facilitated (Ma et al., 2019). A global model represented by the southern German basin, where anoxic conditions (Stages II & III) in bottom and pore waters favored improved organic matter preservation and accumulation due to increased riverine sediment and nutrient delivery from adjacent landmasses, which encouraged marine primary productivity, can support this model. Reduced productivity and increased carbonate precipitation were caused by a brief decline in sea level at the Lower Elegans Bed, which was brought on by slower runoff and recovery of the carbonate factory. A renewed flow of low-salinity arctic water masses via the Viking Corridor and possibly increased freshwater input would promote water column stratification, improved planktonic productivity, and the reestablishment of bottom water anoxia/euxinia (Stages I & II) suggested by increased concentrations of redox-sensitive trace elements above the Lower Elegans Bed.

3. Paleo-productivity

A common indicator of marine primary productivity is element-related, such as Zn, Cu, Ba, Ni, and P. However, the elements P and Ba have significant retention in oxic conditions and are quickly released to the water columns in extremely anoxic conditions (Liu et al., 2019). Additionally, TOC is considered the most accurate measure of primary productivity because it represents the ocean's surface productivity, which appears in the sediment. To measure the paleo-productivity, the proxies' Ni/ Al, TOC, and Ni_{xs}+ Cu_{xs}+ Zn_{xs} are chosen (Ma et al., 2019; Zhang et al., 2019; Wang et al., 2019b; Al-Khatony et al., 2023). The findings indicate that the TOC varies for Ru4 and increases with burial depth for R167, demonstrating that ORS have a clearly higher paleo-productivity than OLS.

The Ni/Al ratios of the ORS range from 14.09 to 34.0 (average 22.52) for well R167. The Ni/Al ratios of the ORS and OLS for well Ru4 range from 13.92 to 25.86 (average 18.30), 6.13 to 19.52 (average 9.94), respectively. The Ni_{xs}+ Cu_{xs}+ Zn_{xs} values of the ORS range from 33.99 to 73.72 (average 49.00) for R167 and ORS and OLS for Ru4 range from 22.14 to 71.18 (average 50.16), 20.35 to 41.06 (average 26.97), respectively. The ORS had greater primary productivity than the OLS, which also suggests that they had higher Ni/Al and Ni_{xs}+ Cu_{xs}+ Zn_{xs} values, which reflect the development and reproduction of organisms in the Lower Cretaceous oceans.

However, there are three distinct decline intervals in Ru4: the first occurs at the depth of Ru4-3, the second between samples Ru4-6 and Ru4-7, and the third is observed at the depth of sample Ru4-11. The TOC, major elements, and redox conditions all changed with these three paleo-productivity reductions. As the first decline progressed from sample Ru4-2 to Ru4-3, TOC reduced from 11.8 to 0.72%, T??Fe₂O₃ and CaO contents **rose** slightly, along with the values of V/Cr and Ni/Co reduced from 2.95 and 7.29 to 2.64 and 5.27, respectively. This indicates an abrupt transition in the environment from euxinic to suboxic conditions. From samples Ru4-5 to Ru4-6 and Ru4-7 at the stage of the second decline, TOC reduced from 6.7 to 0.77 and 0.78%, and the change in major elements is significantly more pronounced than **in** the first decline.

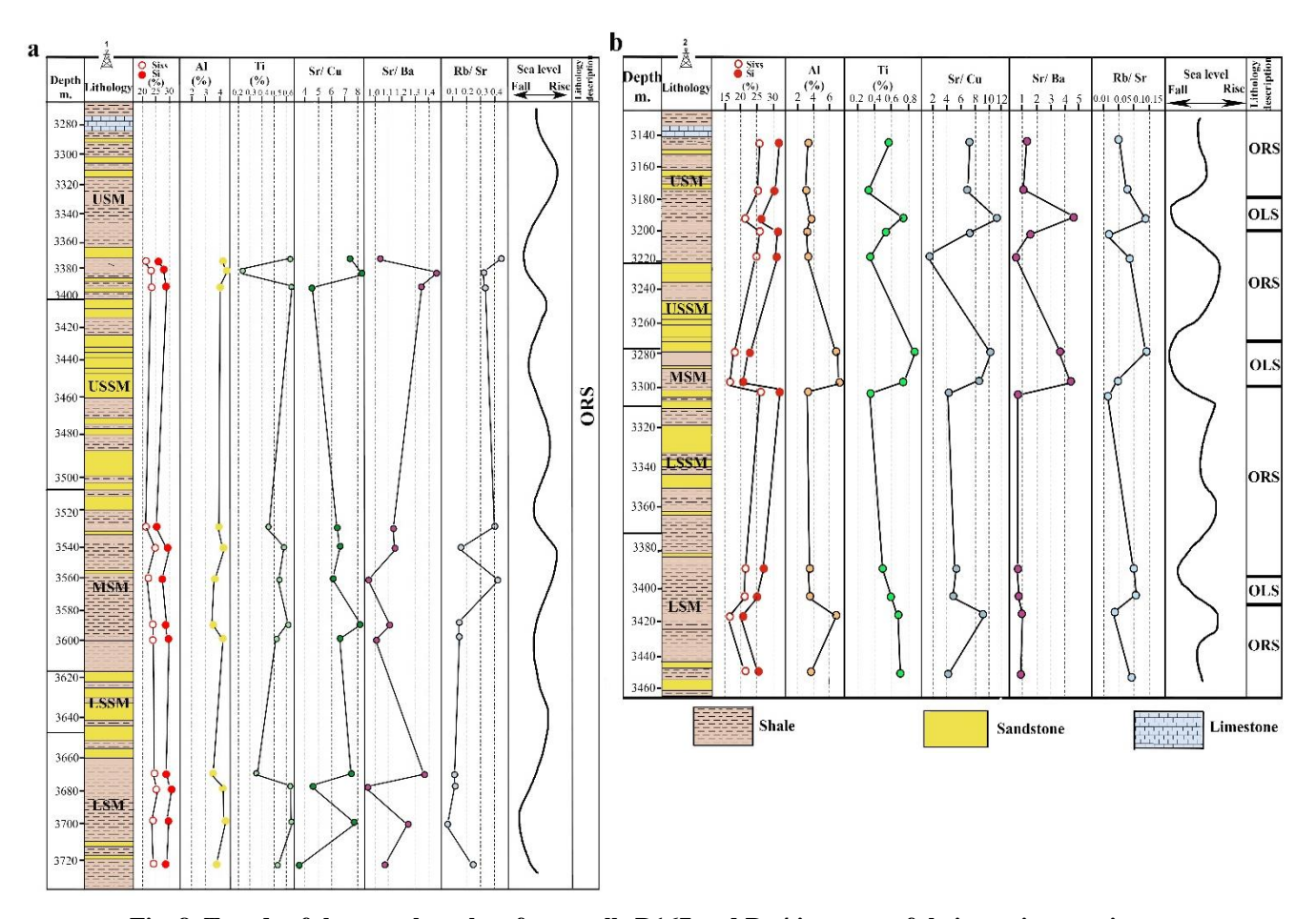


Fig. 8. Trends of the samples taken from wells R167 and Ru4 in terms of their terrigenous input, biological silica, and paleo-climate.

For instance, the content of SiO_2 decreased significantly from 64.33 to 49.72%, and 45.66%, and the content of CaO increased significantly from 0.77 to 3.59%. The V/Cr and Ni/Co ratios dropped from 6.53 and 10.43 to 2.17 and 5.94, respectively, indicating the quick transition from euxinic to suboxic conditions. TOC decreased from 5.7 to 0.75% between samples Ru4-10 and Ru4-11 at the third decline stage, and the reduction in the major elements is significantly greater than the first reduction. For example, the amount of SiO_2 significantly decreased from 54.74 to 46.26%, and Al_2O_3 increased dramatically from 13.65 to 24.32%. As a result of the rapid change from euxinic to suboxic and anoxic conditions, the ratio of V/Cr decreased from 2.82 to 1.77. The study demonstrates that the three reductions in paleoproductivity are linked to rising sea levels. As a result of the sea level dropping, the redox conditions changed from euxinic to suboxic and anoxic, making it difficult for the sulfides, Ni, Zn, and Cu to be deposited and causing a decline in paleo-productivity (Algeo and Liu, 2020; Ibrahim and Abdel Rahman, 2024).

Organic matter accumulation factors

Overall, three factors led to the enrichment in organic matter: 1) the input of organic matter (paleo-productivity), 2) the preservation of organic matter (deposition rates and redox conditions), and 3) the terrigenous detrital input (dilution of organic matter).

Given that shale samples were only chosen to reduce the impact of the lithofacies on the enrichment in organic matter, and that the contents of Al and Ti are noticeably different in these samples. The mean value of La_n/Yb_n in the ORS of R167 is 8.60, and those in the ORS and OLS of Ru4 are 8.61 and 9.36, respectively. This suggests that the ORS have comparatively high deposition rates, which were advantageous for the enrichment in organic matter because they reduced the amount of time of subjection to oxidation. To investigate the variables responsible for organic matter enrichment in the wells R167 and Ru4, relationships between

TOC and the values of Al, Ti, V/ Cr, Ni/ Co, U/Th, δ Ce, Ni/Al, Ni_{xs}+ Cu_{xs}+ Zn_{xs}, and La_n/Yb_n are used. The findings demonstrate that TOC had a significant positive relationship with the proxy for terrigenous detrital input, Al (Fig. 11a), but a weak correlation with Ti (Fig. 11b). TOC had a significant positive relationship with the redox proxies V/Cr (Fig. 11c), Ni/Co (Fig. 11d), U/Th (Fig. 11e), and δ Ce (Fig. 11f). U/Th had the strongest correlation with TOC, followed by Ce, Ni/Co, and V/Cr.

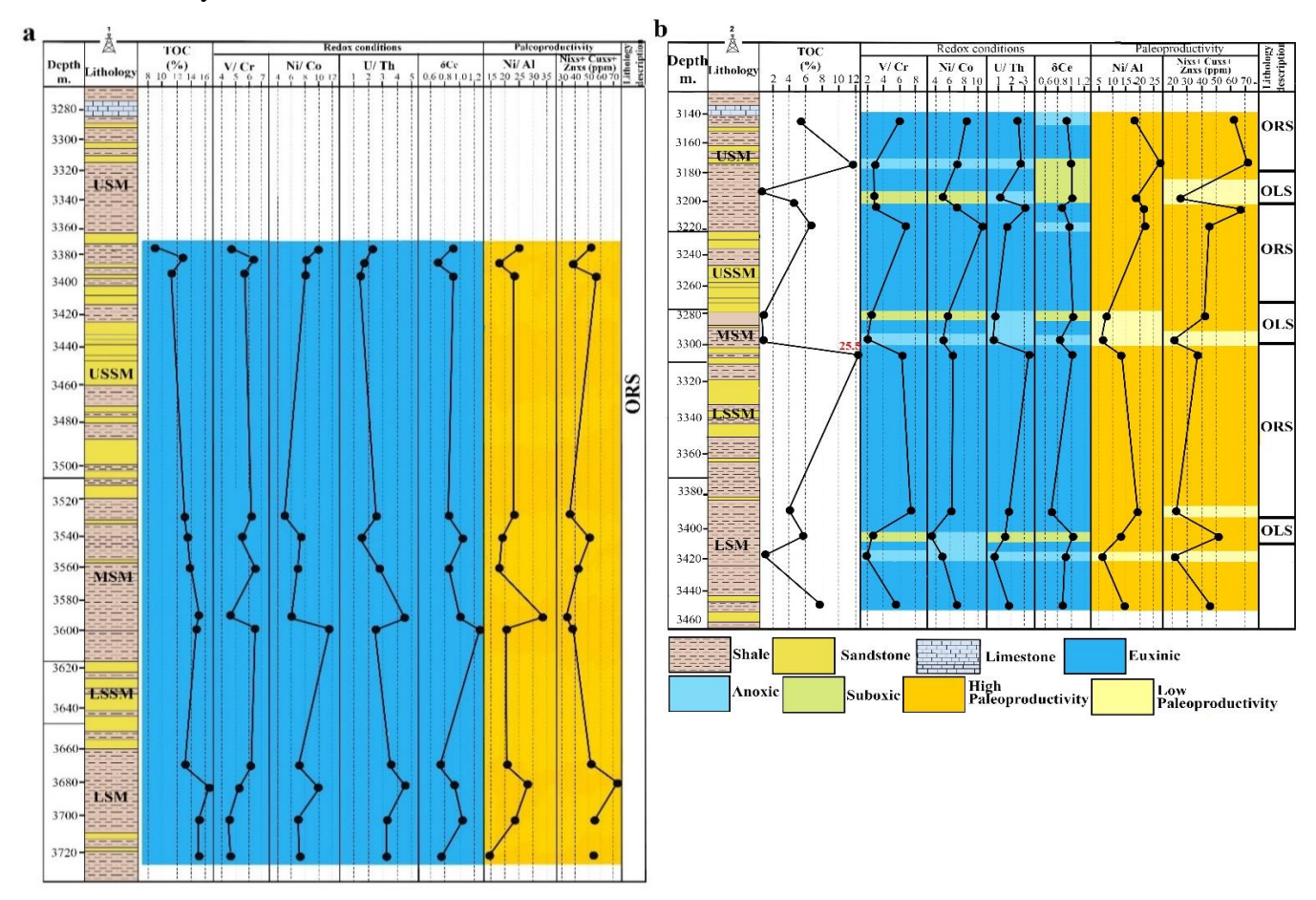


Fig. 9. Stratigraphic distributions for redox conditions (V/Cr, Ni/Co, U/Th, and δ Ce) and paleoproductivity (Ni/Al and Ni_{xs}+ Cu_{xs}+ Zn_{xs}) proxies for the Zubair Shale Formation in wells R167 and Ru4 in (a) and (b), respectively.

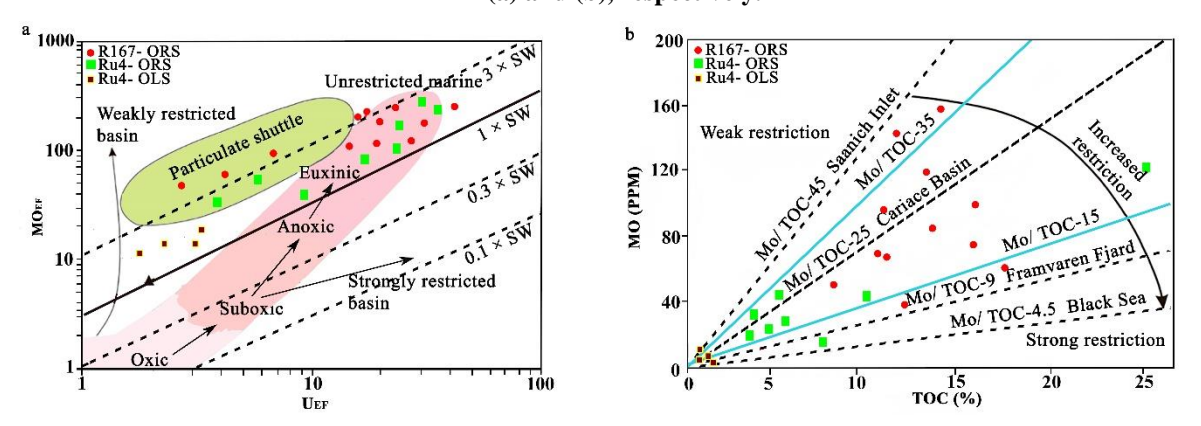


Fig. 10. (a) U_{EF} and Mo_{EF} of samples taken from wells R167 and Ru4 oil shales. (b) Scatter plots of Mo_{EF} vs. TOC for samples of oil shales from wells R167 and Ru4.

The paleoproductivity proxies Ni/Al (Fig. 11g), Ni_{xs}+ Cu_{xs}+ Zn_{xs} (Fig. 11h), and deposition rate proxies La_n/Yb_n (Fig. 11i), all show strong positive correlations with TOC. Detailed investigations demonstrate that terrigenous detrital inputs, redox conditions, paleoproductivity, and deposition rates all affect organic matter content enrichment.

Consistent with the previous studies, paleoredox conditions are the primary controlling factor affecting organic matter enrichment, followed by paleo-productivity and deposition rates. The contribution of terrigenous detritus has a negligible impact on the enrichment of organic matter. The lithology also affects the enrichment of organic matter (Fig. 3). The organic matter content of siliceous shale is highest in ORS (average TOC= 8.96- 13.5%) and lowest in OLS (average TOC= 0.75%).

The model advancement for the Zubair oil shales

The Jurassic and Lower Cretaceous formations in southern Iraq are studied using Type IIS kerogen kinetic to extract the kerogen from the source rocks containing significant amounts of sulfur (nitrogen, sulfur, and oxygen; NSO = 1-34%) (Al-Ameri et al., 2010). An organic matter enrichment model for Zubair oil shales is created for the Rumaila oilfields based on the outcomes of various geochemical proxies (Fig. 12).

Stage I includes rising sea level during deposition of ORS at wells R167 and Ru4 (Figs. 8 and 12a). A warm and humid climate marks the paleo-environment, euxinic conditions with an abundance of free H_2S , a low salinity seawater, terrigenous detrital input, and a comparatively high paleo-productivity, deposition rates, and Si_{xs} content. The marine microorganism development and conservation are great and are beneficial to organic matter enrichment (Schoepfer et al., 2015; Yan et al., 2019). The TOC average values for R167 and Ru4 are 13.5% and 9.04% respectively.

Stage II represents sea level fall and deposition of ORS in Ru4 (Figs. 8 and 12b). A moderately warmer and drier climate, anoxic conditions showing ferrous ions, also medium salinity of seawater and paleo-productivity, higher terrigenous detrital input, and low content of Si_{xs} are the features of the paleo-environment. With a TOC average value of 4.44%, a significant terrigenous detrital input would typically dilute organic matter, which is not favorable for organic matter enrichment.

Stage III is represented by the OLS in the lower, middle, and upper portions of Ru4 and the ongoing decline in sea level (Figs. 8 and 12c). Stage III's paleo-climate changed significantly from Stage II's in terms of temperature and aridity, and seawater salinity. Despite a decrease in the terrigenous detrital input, the bottom water, with a TOC average value of 2.39%, was in suboxic conditions as a result of the level's ongoing decline. This did not support organic matter enrichment.

Increasing seawater depth can also result in less constrained water mass circulation and more nutrients being upwelled to the deep shelf at this stage of sea level rise, which could lead to marine plankton blooms and elevated primary surface productivity (Ma et al., 2019). This process, however, might result in euxinic water conditions and better organic matter conservation (Fig. 12a). In the stage for sea level decrease, the shallow water depth results in more water mass constraints and less effective nutrient upwelling to the deep shelf, both of which were unfavorable to the growth of microorganisms and the increase in primary surface productivity. As for the low stand for sea level, it would result in oxic and suboxic conditions, neither of which are suitable for the survival of microorganisms (Fig. 12b, c).

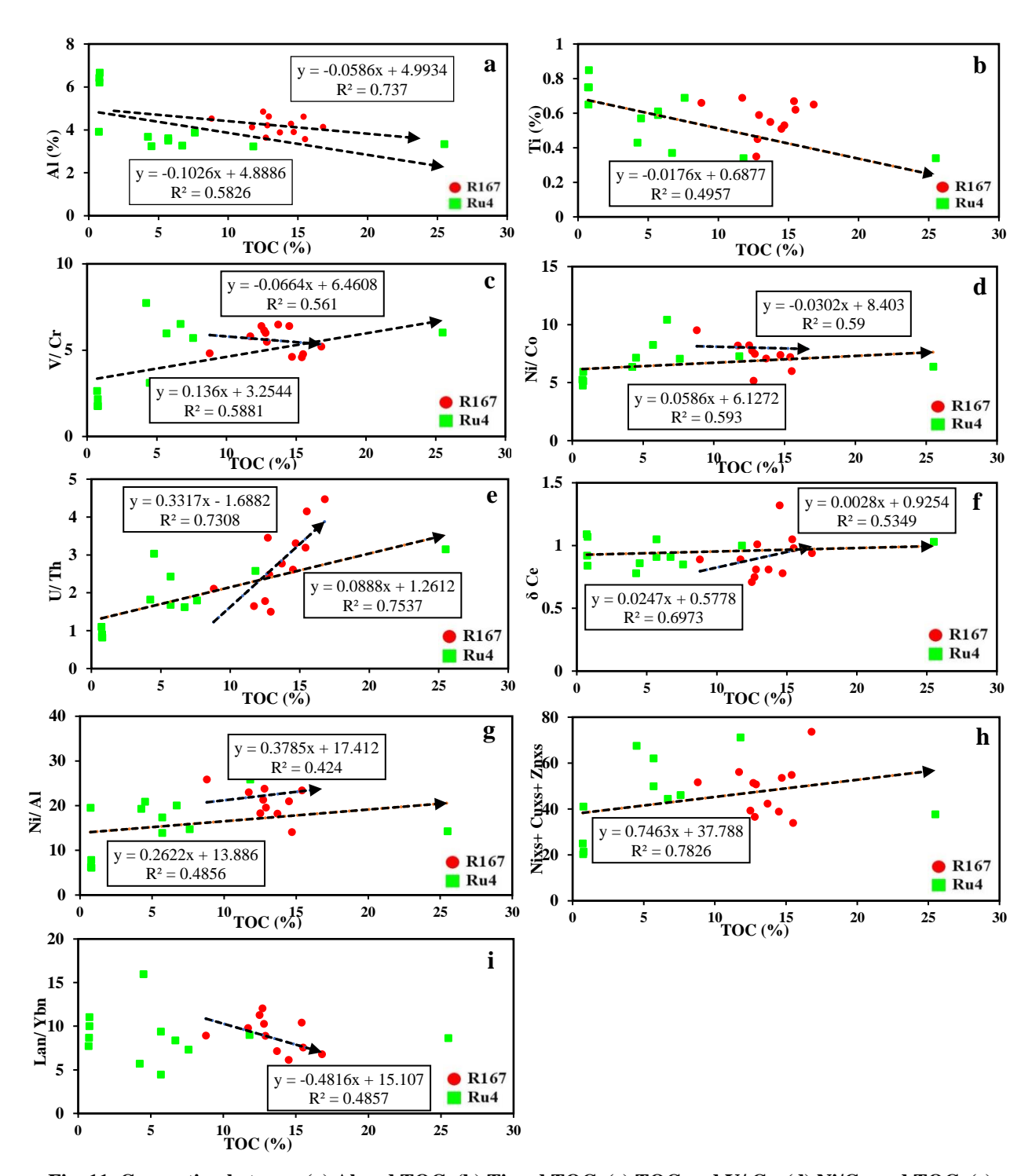


Fig. 11. Connection between (a) Al and TOC. (b) Ti and TOC. (c) TOC and V/ Cr. (d) Ni/Co and TOC. (e) TOC and U/Th. f) TOC and δ Ce. (g) Ni/Al and TOC. (h) Ni_{xs}+ Cu_{xs}+ Zn_{xs} and TOC. (i) La_n/Yb_n and TOC.

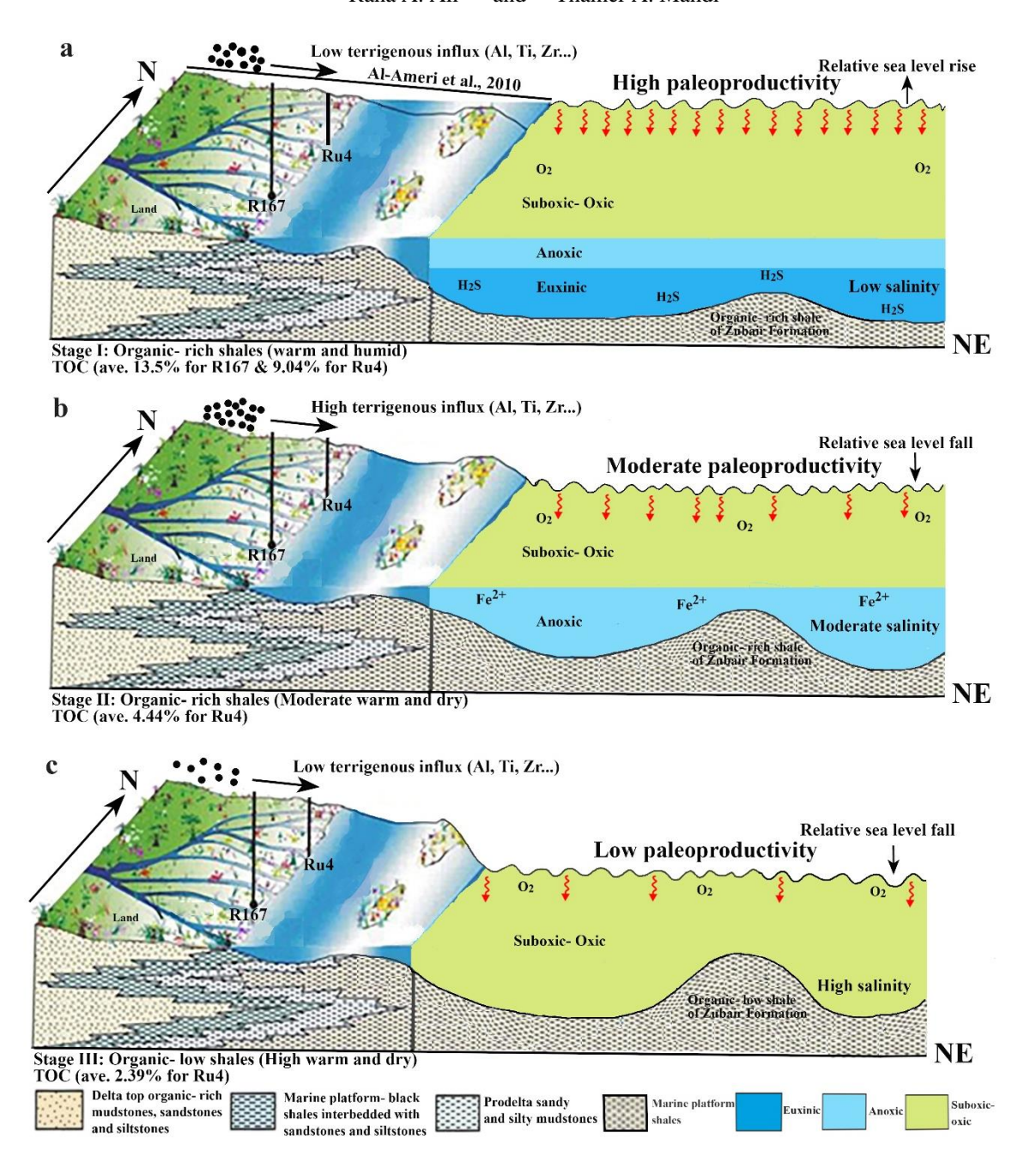


Fig. 12. (a) Model of the R167 and the lower, middle, and upper portions of the ORS of Ru4's organic matter enrichment (Euxinic). (b) Model of the lower, middle, and upper portions of the ORS of Ru4's organic matter enrichment (Anoxic). (c) Model of the lower, middle, and upper portions of the OLS of Ru4's organic matter enrichment (Suboxic).

Conclusions

The Zubair Formation's black shales are separated into ORS and OLS, with average TOC levels of 13.5, 9.04, and 2.39% at wells R167 and Ru4, respectively. The Zubair shales were deposited on the continental margin. They originated from a mix of felsic and intermediate rocks. The ORS contains a higher concentration of biological silica. The OLS have a cold, arid climate with high salinity, while the ORS have a warm, humid climate with low salinity. As a result of the semi-stagnant basin, in which oil shales were deposited, the ORS exhibit a comparatively less stagnant degree, euxinic sulphuretted conditions, and substantial paleoproductivity. The primary element influencing the enrichment of organic matter is the redox condition. Three stages of the Zubair oil shale's organic matter enrichment can be distinguished: the early stage is characterized by a warm, humid climate, high paleoproductivity, and euxinic conditions. The middle stage shows anoxic ferruginous conditions and a warm and dry climate

with a moderate level of paleo-productivity. The late stage is distinguished by suboxic to oxic conditions, a less warm and drier climate, and a fairly low paleo-productivity. The highest quality layer for shale oil exploration, according to this study, is the siliceous shale in the R167 and Ru4 of the ORS, which have thicknesses of about 270 and 200 m and average TOC values of 13.5 and 9.04% respectively.

Funding sources

This research received no specific grant from funding agencies in the public, commercial, or not-for-profit sectors.

Acknowledgements

The authors appreciate the Basra Oil Company and the Iraqi Oil Exploration Company for providing the necessary information and cores. Sincere thanks go to the laboratory workers who carried out the experiments.

Conflict of Interest

The authors declare that there are no conflicts of interest regarding the publication of this manuscript.

References

- Al-Ameri, T.K., Pitman, J., Naser, M.E., Zumberge, J., Al-Haydari, H.A., 2010. Programmed oil generation of the Zubair Formation, Southern Iraq oilfields: results from PetroMod software modeling and geochemical analysis. Arab. Journ. of Geosciences, 4 (7-8), pp. 1239–1259. https://doi.org/10.1007/s12517-010-0160-z.
- Al-Azzawi, R.M.I., 2012. The petroleum system of Zubair Formation in selected oil fields-Southern Iraq. PhD, Baghdad University, Baghdad, Iraq (in English), p. 200.
- Algeo, T.J., Tribovillard, N., 2009. Environmental analysis of paleoceanographic systems based on molybdenum-uranium covariation. Chemi. Geol., 268 (3), pp. 211–225. Doi: 10.1016/j.chemgeo.2009.09.001.
- Algeo, T.J., Liu, J., 2020. A re-assessment of elemental proxies for paleoredox analysis. Chem. Geol., 540, 119549. https://doi.org/10.1016/j.chemgeo.2020.119549.
- Al-Khatony, F.H., AL-Hamidi, R.I., Al-Lhaebi, S.F., 2023. Paleoenvironmental Conditions of the Chia Gara Formation from Rania Section North Eastern Iraq Using Geochemical Constraints. Iraqi National Journal of Earth Science, Vol. 23, No. 1, pp. 154-167. DOI: 10.33899/earth.2023.139987.1078
- Ali, R.A., Jassim, H.K., 2023. Sedimentology and geochemistry of Zubair Formation sandstone reservoir, East Baghdad Oilfield, central Iraq. Kuwait Journal of Science, 50(3), pp. 427-437. https://doi.org/10.1016/j.kjs.2023.01.006
- Ali, R. A., 2023. Petrography and geochemistry of Zubair Shale Formation in Rumaila Oilfield, Southern Iraq: Implications for provenance and tectonic setting. J. of Petroleum Research and Studies, 13 (3): 40, pp. 19- 40. https://doi.org/10.52716/jprs.v13i3
- Alsultan, H.A.A., Awadh, S.M., Al-Owaidi, M.R.A., Al-Khafaji, A.J., 2021. Sequence Stratigraphy and Depositional Environment of the Zubair Formation in Rumaila Oilfields, Southern Iraq: Microfacies and Geochemistry. Iraqi Geological Journal, 54 (2B), pp. 28-41. DOI:10.46717/igj.54.2B.3Ms-2021-08-23
- Buday, T., 1980. The Regional Geology of Iraq: Stratigraphy and Palaeogeography. State Organisation for Minerals Library, Baghdad, Iraq, Vol. 1, 445 P.

- Chen, Y., Zhu, Z., Zhang, L., 2019. Control actions of sedimentary environments and sedimentation rates on lacustrine oil shale distribution, an example of the oil shale in the Upper Triassic Yanchang Formation, southeastern Ordos Basin (NW China). Mar. Pet. Geol., 102, pp. 508–520. DOI: 10.1016/j.marpetgeo.2019.01.006
- Davies, R.B., Casey, D.M., Horbury, A.D., Sharland, P.R., Simmons, M.D., 2002. Early to mid-Cretaceous mixed carbonate-clastic shelfal systems: examples, issues and models from the Arabian Plate. Geo Arabia, 7 (3), pp. 541-598. https://doi:10.2113/geoarabia0703541.
- Doner, Z., Kumarl, M., Demirel, I. H., Hu, Q., 2018. Geochemical characteristics of the Silurian shales from the central Taurides, southern Turkey: organic matter accumulation, preservation and depositional environment modeling. Marine and Petroleum Geology, 102, pp. 155–175.DOI: 10.1016/j.marpetgeo.2018.12.042
- Fang, Y., Su, J., Wang, X., Ma, S., Yang, C., Zhang, S., 2023. The transition from hydrothermal oxic conditions to restricted euxinia in the Lower Cambrian Yurtus Formation black shale, Tarim Basin. Marine and Petroleum Geology, 156, 106420. https://doi.org/10.1016/j.marpetgeo.2023.106420
- Fathy, D., Wagreich, M., Ntaflos, T., Sami, M., 2021. Paleoclimatic variability in the southern Tethys, Egypt: insights from the mineralogy and geochemistry of upper Cretaceous lacustrine organic-rich deposits. Cretaceous Research, 126, 104880. Doi: 10.1016/j.cretres.2021.104880
- Fonseca, R., Araújo, J.F., Pinho, C.G., 2021. Importance of the Spatial Distribution of Rare Earth Elements in the Bottom Sediments of Reservoirs as a Potential Proxy for Tracing Sediments Sources. A Case Study in the Dominican Republic. Geosciences, 11 (490), pp. 1-27. https://doi.org/10.3390/geosciences11120490.
- He, L., Wang, Y., Chen, D., Wang, Q., Wang, C., 2019. Relationship between sedimentary environment and organic matter accumulation in the black shale of Wufeng- Longmaxi Formations in Nanchuan area, Chongqing. Jou. of Natu. Gas Geoscience, 30, pp. 203–218.
- Ibrahim, K.M. and Abdel Rahman, H.B., 2024. Uranium and Organic Geochemistry of Oil Shale in Attarat Um Ghudran, Jordan. Iraqi National Journal of Earth Science, 24(1), pp.271-289.https://10.33899/earth.2023.142670.1133.
- Idan, R.M., Faisal, R.F., Nasser, M.E., Al-Ameri, T.K., Al-Rawi, D., 2014. Hydrocarbon potential of Zubair Formation in the south of Iraq. Arab. J. Geosci., 8 (7), pp. 4805-4817. https://doi:10.1007/s12517-014-1569-6.
- Idan, R.M., Al-Musawi, F.A., Salih, A.L., Al-Qaraghuli, S.A., 2019. The petroleum system of Zubair Formation in Zubair Subzone, Southern Iraq. Jou. of Petroleum Rese. & Studies, 25 (12), pp. E57- E73. https://doi.org/10.52716/jprs.v9i4.322
- Janssen, M., Caracciolo, L., Bonnell, L.M., Lander, R.H., et al., 2023. Climatic, depositional and environmental controls on early carbonate cementation in fluvial and shallow marine sandstones. Marine and Petroleum Geology, 106433 (in Press). https://doi.org/10.1016/j.marpetgeo.2023.106433
- Li, Y., Zhang, T., Ellis, G.S., Shao, D., 2017. Depositional environment and organic matter accumulation of Upper Ordovician-Lower Silurian marine shale in the Upper Yangtze Platform, South China. Palaeogeography, Palaeoclimatology, Palaeoecology, 466, pp. 252–264. https://doi.org/10.1016/j.palaeo.2016.11.037

- Liao, Z., Hu, W-X., Fu, X-G., Hu, Z., 2018. Geochemistry of upper Permian siliceous rocks from the Lower Yangtze region, southeastern China: implications for the origin of chert and Permian Ocean chemistry. Petroleum Science, 16 (1). https://doi:10.1007/s12182-018-0293-3
- Liu, W., Yao, J., Tong, J., Qiao, Y., Chen, Y., 2019. Organic matter accumulation on the Dalong Formation (Upper Permian) in western Hubei, South China: constraints from multiple geochemical proxies and pyrite morphology. Palaeogeography, Palaeoclimatology, Palaeoecology, 514, pp. 677–689. https://doi:10.1016/j.palaeo.2018.11.015
- Liu, P., Liu, C., Guo, R., 2023. Depositional Environment and Organic Matter Enrichment in the Lower Paleozoic Shale from the Northeastern Margin of the Yangtze Platform, South China. Journal of Marine Science and Engineering, 11 (501). https://doi.org/10.3390/jmse11030501
- Ma, Y., Lu, Y., Liu, X., Zhai, G., Wang, Y., Zhang, C., 2019. Depositional environment and organic matter enrichment of the lower Cambrian Niutitang shale in western Hubei Province, South China. Marine and Petroleum Geology, 109, pp. 381–393. https://doi.org/10.1016/j.marpetgeo.2019.06.039
- Mahmoud, A.I., Metwally, A.M., Mabrouk, W.M., Leila, M., 2023. Controls on hydrocarbon accumulation in the pre-rift paleozoic and late syn-rift cretaceous sandstones in PTAH oil field, north Western Desert, Egypt: Insights from seismic stratigraphy, petrophysical rock-typing and organic geochemistry. Marine and Petroleum Geology, 155, 106398. https://doi.org/10.1016/j.marpetgeo.2023.106398
- McLennan, S.M., 2001. Relationships between the trace element composition of sedimentary rocks and upper continental crust. Geochemistry, Geophysics, Geosystems, 2. https://doi:10.1029/2000gc000109
- Schoepfer, S.D., Shen, J., Wei, H., Tyson, R.V., Ingall, E., Algeo, T.J., 2015. Total organic carbon, organic phosphorus, and biogenic barium fluxes as proxies for paleomarine productivity. Earth-Science Reviews, 149, pp. 23–52. https://doi:10.1016/j.earscirev.2014.08.017
- Shen, J., Zhou, L., Feng, Q., Zhang, M., Lei, Y., Zhang, N., Yu, J., Gu, S., 2014. Paleo-productivity evolution across the Permian-Triassic boundary and quantitative calculation of primary productivity of black rock series from the Dalong Formation, South China. Science China Earth Sciences, 57, pp. 1583–1594. https://doi.org/10.1007/s11430-013-4780-5
- Wang, Z., Wang, J., Fu, X., Zhan, W., Yu, F., Feng, X., Song, C., Chen, W., Zeng, S., 2017. Organic material accumulation of Carnian mudstones in the North Qiangtang Depression, eastern Tethys: controlled by the paleoclimate, paleoenvironment, and provenance. Marine and Petroleum Geology, 88, pp. 440–457. https://doi.org/10.1016/j.marpetgeo.2017.08.029
- Wang, X., Zhu, Y., Lash, G.G., Wang, Y., 2019a. multi-proxy analysis of organic matter accumulation in the Upper Ordovician-Lower Silurian black shale on the Upper Yangtze Platform, south China. Marine and Petroleum Geology, 103, pp. 473–484. https://doi.org/10.1016/j.marpetgeo.2019.03.013
- Wang, Y., Xu, S., Hao, F., Lu, Y., Shu, Z., Detian, Yan, D., Lu, Y., 2019b. Geochemical and petrographic characteristics of Wufeng- Longmaxi shales, Jiaoshiba area, southwest China: Implications for organic matter differential accumulation. Marine and Petroleum Geology, 102, pp.138-154. https://doi.org/10.1016/j.marpetgeo.2018.12.038

- Wu, W., Liu, W., Mou, C., Liu, H., Qiao, Y., Pan, J., Ning, S., Zhang, X., Yao, J., Liu, J., 2021. Organic-rich siliceous rocks in the upper Permian Dalong Formation (NW middle Yangtze): Provenance, paleoclimate and paleoenvironment. Marine and Petroleum Geology, 123, 104728. https://doi.org/10.1016/j.marpetgeo.2020.104728
- Xu, L., Huang, S., Liu, Z., Zhang, Y., Wen, Y., Zhou, X., Chen, W., Ren, Z., Wen, J., 2022. Paleoenvironment evolutionary characteristics of Niutitang shale in Western Hubei, Middle Yangtze, China. ACS Omega, 7, pp. 24365–24383. https://doi.org/10.1021/acsomega.2c01726
- Yan, C., Jin, Z., Zhao, J., Du, W., Liu, Q., 2018. Influence of sedimentary environment on organic matter enrichment in shale: A case study of the Wufeng and Longmaxi Formations of the Sichuan Basin, China. Marine and Petroleum Geology, 92, pp. 880–894. https://doi.org/10.1016/j.marpetgeo.2018.01.024
- Yan, D., Chen, D., Wang, Z., Li, J., Yang, X., Zhang, B., 2019. Climatic and oceanic controlled deposition of Late Ordovician-Early Silurian black shales on the North Yangtze platform, South China. Marine and Petroleum Geology, 110, pp.112–121. https://doi.org/10.1016/j.marpetgeo.2019.06.040
- Zhang, L., Xiao, D., Lu, S., Jiang, S., Lu, S., 2019. Effect of sedimentary environment on the formation of organic-rich marine shale: Insights from major/trace elements and shale composition. International Journal of Coal Geology, 204, pp. 34–50. https://doi:10.1016/j.coal.2019.01.014
- Zhang, K., Li, X., Wang, Y., Liu, W., Yu, Y., Zhou, L., Feng, W., 2021. Paleo-environment sand organic matter enrichment in the shales of the Cambrian Niutitang and Wunitang Formations, south China: Constraints from depositional environments and geochemistry. Marine and Petroleum Geology, 134, 105329. https://doi:10.1016/j.marpetgeo.2021.105329